NUMERICAL MODELLING OF AN OSCILLATORY BAFFLED COLUMN

by

Case W. Bakker

Dissertation presented to the University of Cape Town for the degree of Master of Science in the Department of Mechanical Engineering

Supervisors:

Dr C.J. Meyer

Dr D. Deglon

Department of Mechanical Engineering

University of Cape Town

November 2005

Declaration

I, Case William Bakker, hereby declare that this thesis is my own work and that it has not been submitted for a degree at any other university

…….. ……

Case William Bakker Date

Abstract

Since the flotation process was initially developed, the traditional impeller driven flotation cell has been almost exclusively used. A relatively new mixing cell that has found to have many advantages over the impeller driven cells is the Oscillatory Baffled Column (OBC). The aim of this project was to develop a numerical model to resolve the flow field in a general OBC. This model can then later be modified to be used to model the more complex OBC that is presently being experimentally tested by the Mineral Processing Research Unit at the University of Cape Town.

The commercial CFD code FLUENT 6.2.16 was used to create the model. Numerical simulations were conducted to investigate the effects of different methods of defining the oscillatory flow, using both RANS turbulence models and Large Eddy Simulation (LES) to model turbulence, as well as different grid sizes and different discretization schemes. The results were validated using Digital Particle Image Velocimetry (DPIV) results of phase averaged velocity magnitude, turbulent kinetic energy (TKE) and turbulence integral length scale found in literature.

All simulations performed used a second order implicit temporal scheme with a time step of 0.005s. It was found that the most appropriate method of defining the oscillatory flow was by using translational periodic boundary conditions, together with a journal file to reset the sinusoidally oscillating mass flow rate. Large Eddy Simulation (LES) was chosen to be used in all simulations.

All 3 grid sizes used, which ranged from 551 225 to 726 804 cells, gave approximately the same phase averaged velocity magnitude, turbulent kinetic energy and energy dissipation rate. It was therefore decided that a grid of 551 225 cells was adequate to model the OBC. The Dynamic Smagorinsky-Lilly subgrid-scale model was chosen to be used in all simulations, as well as the SIMPLEC pressure-velocity coupling scheme, and the Standard pressure discretization scheme.

The momentum discretization scheme had a large effect on the results, with the Central Differencing scheme predicting that the flow became asymmetric sooner than any of the other schemes with transportive properties, such as the QUICK or Bounded Central Differencing Schemes. The QUICK momentum discretization scheme was decided to be the most appropriate scheme. It was found that both discretization schemes and subgrid-scale models had no significant effect on phase averaged mean velocity magnitude, and little effect on phase averaged mean turbulent kinetic energy.

Acknowledgements

- Mineral Processing Research Unit (MPRU) and Center for Research and Applied Mechanics (CERECAM) at the University of Cape Town for financial support
- My supervisor, Dr. Chris Meyer. His enthusiasm and guidance, as well as his knowledge during this project was greatly appreciated.
- My co-supervisor, Dr. Dave Deglon for his invaluable advice and guidance
- My father and brothers, as well as the rest of my extended family for all their support throughout my studies.
- Last, but not least, my friends for their encouragement.

Table of Contents

Table of Figures

Nomenclature

Abbreviations

BCD	Bounded Central Differencing
CBC	Convection Boundedness Condition
CD	Central Differencing
CFD	Computational Fluid Dynamics
CFL	Courant-Friedrich-Levy
DPIV	Digital Particle Image Velocimetry
LES	Large Eddy Simulation
OBC	Oscillatory Baffled Column
RANS	Reynolds Averaged Navier-Stokes
RSM	Reynolds Stress Model
SGS	Subgrid-scale
TKE	Turbulent Kinetic Energy
UDF	User Defined Function

Symbols

u'	Fluctuating velocity component (m/s)
$\overline{u}$	Resolved velocity in LES (m/s)
u''	Subgrid, or unresolved velocity in LES (m/s)
$\dot{m}$	Mass flow rate (kg/s)
C_s	Smagorinsky constant (= 0.1)
D	Column Diameter (mm)
d	Distance to closest wall (m)
D_o	Orifice Diameter (mm)
f	Oscillating Frequency (Hz)
g	Gravitational acceleration (m/s^2)
k	Turbulent Kinetic Energy (m^2/s^2)
l	Turbulent integral length scale (m)
L	Baffle spacing (mm)

L_s	Mixing length (m)
p	Pressure (N/m^2)
Re_n	Net flow Reynolds Number
Re_o	Oscillatory Reynolds Number
S_{ij}	Strain rate tensor (s^{-1})
St	Strouhal number
t	Time (s)
u_i	Instantaneous velocity (m/s)
u_m	Mean velocity component (m/s)
x_o	Oscillation amplitude (mm) (Centre to Peak)
y^+	Wall unit

Greek Symbols

ε	Dissipation rate (m^2/s^3)
κ	von Kàrmàn constant (= 0.42)
μ	Fluid viscosity (kg/ms)
μ_t	Subgrid-scale turbulent viscosity (kg/ms)
ν	Kinematic viscosity (m^2/s)
ρ	Fluid density (kg/m^3)
τ_w	Wall shear stress (m^2/s^2)
τ_{ij}	Subgrid-scale Reynolds stress (m^2/s^2)

1. Introduction

1.1 Background

The mining industry is one of the cornerstones of South Africa's economy. South Africa is one of the worlds biggest producer of gold and platinum, as well as one of the leading producers of various other base metals, and exports mineral commodities to 80 countries worldwide. One of the most widely used methods to separate these metal-bearing minerals from the rest of the ore is by the use of the froth-flotation process.

This process entails first milling the ore into a fine powder and mixing it with water, forming slurry. Frothing and collecting reagents are then added, making the mineral-bearing particles hydrophobic, and the rest of the particles hydrophilic. This mixture is then agitated by various means, while air bubbles are dispersed through the mixture. The hydrophobic mineral particles attach to the bubbles, which rise to form a froth on the surface. The froth is then removed as clean mineral concentrate, while the waste material, called gangue, is removed from the vessel as a slurry.

The method traditionally used to agitate the slurry mixture is by using an impeller driven mixing cell. A relatively new and novel method used for agitating the slurry is by using a type of oscillatory baffled column, or OBC. The OBC currently being tested by Chris Anderson and Dr. Dave Deglon of the Mineral Processing Research Unit (MPRU) at the University of Cape Town consists of a standard column section containing a sinusoidally oscillating baffle cage with baffles transverse to the fluid flow that can be operated at a variety of amplitudes and frequencies and was developed in collaboration with Dr. Paul Stonestreet of Cambridge University. There is also a net through-flow through the column. As the liquid flows past the baffles in the column, bounded vortices form downstream of the baffles. As the flow reverses in direction, these vortices get swept back into the bulk of the liquid, interacting with other vortices, thereby creating a highly mixed flow. This allows OBC's to thoroughly mix fluids (1989BR01).

The flow conditions inside OBC's are defined by 3 main dimensionless numbers (2003NI01):

- Oscillatory Reynolds number (Re_o)

  This describes the intensity of mixing applied to the column, and is defined by Eq. 1.1

$$\mathrm{Re}_o = \frac{2\pi x_o f \rho D}{\mu} \tag{1.1}$$

  Where x_o is the centre to peak amplitude (m), f is the oscillation frequency (Hz), ρ is the fluid density ($kg\ m^{-3}$), D is the column diameter (m), and μ is the fluid viscosity ($kg(ms)^{-1}$)

- Net flow Reynolds number (Re_n)

$$Re_n = \frac{\rho u D}{\mu} \tag{1.2}$$

  This is the same as the Reynolds number used in steady flow and defines the net flow through the column.

- Strouhal number (St).

  This defines the ratio of the column diameter to stroke length, measuring the effective eddy propagation and is defined by Eq. 1.3

$$St = \frac{D}{4\pi x_o} \tag{1.3}$$

There are also two other geometrical parameters: the baffle spacing (L/D), and the baffle free area ($\alpha = D_o/D$)

One of the main advantages of the OBC over the impeller driven vessels is that it can achieve more uniform shear rates (2004CH01), and for this reason and others it has achieved successes in various other industries, including particle flocculation, bead polymerization, crystallization and bio-processing.

To optimize the flotation process, the flow inside the column must be understood. It is known that energy input plays an important role in the flotation performance in conventional impeller driven flotation cells, but with the OBC, different combinations of oscillating frequency and amplitudes can produce the same energy input, and it is unknown whether these different combinations will produce similar flows, i.e. similar distribution of local energy dissipation rates. It has been hypothesized by Chris Anderson that the flotation performance of OBC's is dependent on the distribution of local energy dissipation rates, and not the overall energy input.

Experimental methods that can be used to calculate local energy dissipation rates, such as Digital Particle Image Velocimetry (DPIV), are expensive. An alternative is to create a numerical model to predict these distributions using Computational Fluid Dynamics (CFD). Not only would this be less expensive, it would eliminate the need for new experimental models to be constructed if the OBC geometry is modified.

1.2 Theoretical Approach

Rather than trying to model the complex OBC that is being tested by Chris Anderson, the flow inside a basic OBC was simulated to validate the numerical model. This OBC was used by Prof. X. Ni and his colleagues from Heriot-Watt University in Edinburgh in his research (2000NI01, 2002NI01, 2003NI01, 2003FI01, 2003JI01). Rather than oscillating the baffles, in this model the baffles are fixed to the wall of the column and the fluid is oscillated instead. There is also no net flow through the column, therefore $Re_n = 0$. Experimental DPIV data as well as numerical data are available, providing a comparison for CFD results. Once an accurate model of the simpler OBC has been created, it is

thought that it will be a relatively easy exercise to modify the model to represent the novel OBC.

1.3 Scope of Thesis

This research was initiated with the aim to improve the understanding of the flow dynamics inside an oscillatory baffled column, and to investigate the flotation performance of the OBC and the factors that affect this in order to optimize it.

The aim of this research is to develop a numerical model to resolve the flow field inside an OBC that is both numerically and physically accurate, and to then validate this with experimental data available in literature. This methodology can later be used to create a numerical model of the OBC currently being tested by Chris Anderson, and predict local energy dissipation rate distributions at various frequency and amplitude combinations.

2. An Overview of Numerical and Experimental Research in Oscillatory Baffled Columns

Research first began into understanding and optimizing the flow in baffled columns about 70 years ago, but it has only been in the last 20 or so years that any research has been conducted on baffled columns with oscillatory flow. Below is a summary of the research that has been conducted to understand the flow inside an OBC. Although there have been other studies on OBC's, only the ones that will contribute to the development of a numerical model have been included.

2.1 Experimental Research

Brunold *et al* (1988BR01) was first to conduct experimental research into oscillatory flow on columns with sharp edged baffles. A circular column was used with a diameter of 46mm, having either one or two baffles, with the distance between the baffles varied when two baffles were used, and particle image velocimetry (PIV) was used to visualize the flow. It was found that the flow behind each baffle in the column was the same, and therefore the flow should be the same for any number of baffles. It was also found that the baffle spacing had an effect on the mixing in the column. The spacing found to give the most mixing was 1 ½ times the column diameter, and this ratio has been used in all subsequent research.

Mackley and Ni (1991MA01) studied the dissipation in OBC's using a salt solution tracer and the concentration, and therefore the dissipation of the tracer, was measured along the column first on its side, and then upright. This was done by using conductivity probes placed along the length of the column. The salt solution was injected into the one end of the column, and the salt concentrations where then measured with respect to time. This allowed the residence time of the salt solution to be measured. It was found that even small density differences between the tracer and bulk fluid made a large difference to the concentration profile, and that OBC's provided excellent radial mixing.

Roberts and Mackley (1996RO01) conducted both experimental research and numerical modelling of oscillatory flow in a rectangular baffled channel. The numerical modelling will be discussed in Section 2.2. PIV was used to visualize the flow with relatively large oscillation amplitudes (19.9-59.6mm) and low frequencies (1-2.2Hz). They found experimentally that for their rectangular column, the flow began to become three dimensional at a Re_o number in the order of 100 for all the St numbers tested, ranging from 1 to 0.341. When the flow becomes asymmetric at Re_o =150-200, the large scale structures in the flow were found to be highly periodic, but the level of asymmetry would tend to change after 10 cycles or more. It was also observed that the critical Re_o number for asymmetry, i.e. the Re_o number where the flow begins to become asymmetric, increases with decreasing St number.

Ni (1999NI01) also studied the strain rates inside OBC's using PIV for further studies into flocculation using OBC's. The OBC used had a column diameter of 50mm and orifice diameter of 23mm. Re_o numbers of 251-4021 were used. Ni (1999NI01) found that the strain rates in OBC's were lower than stirred vessels, which are traditionally used for flocculation. Instantaneous strain-rate maps, phase averaged velocity vector maps, as well as values of volume averaged strain rates and variance of strain rates were calculated, and are available. It was also found that for the OBC geometry used in this study, the flow became asymmetric at Re_o>1580.

Fitch and Ni (2003FI01) then conducted a second study investigating mixing in OBC's using laser induced fluorescence (LIF). This was done by injecting a dye into the column that fluoresces when induced by a laser. The intensity of the fluorescence corresponds to the concentration of the dye, so the concentration of the dye, and therefore the amount of mixing can be measured. This method was an advantage over the tracer method since the concentration could be measured at any point in the column, unlike the tracer method, where it could only be measured where the conductivity probes were. Therefore by using LIF, the amount of dispersion could be measured both axially and radially. The results

obtained using this method compared well with the results obtained using the traditional tracer method.

2.2 Numerical Modelling

As mentioned earlier, Roberts and Mackley (1996RO01) also used a numerical model of the OBC used in the experimental research. All the simulations used a 2D laminar model, with the volumetric oscillatory flow being created by making both the axial and radial velocity, as well as the stream function at either end of the column equal and varying the stream function with time. Although the flow became 3D at relatively low Re_o numbers, and therefore the 2D laminar model could not be directly compared to the experimental results, it was thought that there was a possible link between 2D stability behavior and 3D transitions, providing a reason for the modelling.

The flow was first restricted to be symmetrical by the use of a centerline symmetry constraint, and then later relaxing the constraint, allowing the flow to become asymmetric. The degree of asymmetry was measured using a parameter, λ, which is the mean absolute value of the cross channel velocity on the centerline. It was found that λ increased linearly for the first 50 cycles, and after around 65 cycles λ remained constant, meaning the flow had reached a fully saturated asymmetric state. It was also found that it could take many hundreds of cycles for the flow to become fully developed.

Ni (2002NI01) used a numerical model created using *FLUENT 5* to simulate the flow inside a circular OBC, the same OBC as used in his other studies (1999NI01, 2003FI01). The model was validated by comparison to experimental research using digital particle image velocimetry (DPIV). It was assumed that the flow was spatially periodic between baffles, and therefore only 2 baffles were modeled, along with 1 baffle spacing on either end. Both 2D and 3D models were used, the first time a 3D numerical model has been used to model OBC's.

Laminar simulations were carried out using the 2D model at Re_o of 312 (x_0 = 2mm,

f = 0.5Hz) and 1250 (x_0 = 4mm, f = 1Hz), and close correlation was found at Re_o = 312, but the results deviated significantly from the experimental results at the higher Re_o. The model used was not an axisymmetric model though, and therefore essentially had an infinite length in the z direction, i.e. it modeled a rectangular column, and therefore cannot be used to accurately model the flow in a circular OBC.

A 3D model using a structured mesh with 155 198 cells was used to perform laminar simulations at the same Re_o numbers, and showed a close visual correlation to the experimental results at both Re_o numbers, with the flow at Re_o = 1250 showing some asymmetry, even though in previous research it was stated that asymmetry only occurs at Re_o>1580 (1999NI01).

Ni (2002NI01) also used large eddy simulation (LES) to model the OBC oscillating at Re_o = 1250. The RNG-based subgrid-scale model was used with an unstructured, hexahedral mesh of 362 712 cells, and using a time step of 0.0125s. It was found that there was little true turbulence at that Re_o number, shown by the very low subgrid turbulent kinetic energy, and that the global laminar unsteadiness is largely responsible for the uniform mixing conditions in the OBC.

Jian and Ni (2003JI01) then modeled the flow inside the same OBC at Re_o =2500 (x_o = 4mm, f = 2Hz). DPIV data showed that at that Re_o the flow was both turbulent and asymmetric. Both Reynolds Averaged Navier Stokes (RANS) turbulence models and LES were used and the results compared with experimental results from DPIV. The RNG k-ε turbulence model was used to represent RANS models, using non-equilibrium wall functions to model the near-wall region. It was not mentioned how large the mesh used was, apart from the fact that $y^+ \sim 30$, where y^+ is defined as follows

$$y^+ = \frac{\Delta y_P}{\nu}\sqrt{\frac{\tau_w}{\rho}} \qquad (2.2.1)$$

with Δy_P being the distance of the wall node P to the solid surface, and τ_w the wall shear stress.

It was found that although the DPIV results showed chaotic and asymmetric flow, the numerical model predicted highly symmetric flow with strong axial velocity, which was attributed to the Reynolds averaging process within the RANS models, which smoothes out the turbulence in such flows, and it was therefore concluded that RANS models were not suitable to model the flow in OBC's. An unstructured, hexahedral mesh of 780 040 cells was used for LES simulation, making sure that $y^+ \sim 1$, with a time step of 0.0125s, which was small enough to satisfy the Courant-Friedrichs-Levy (CFL) condition ($N_{CFL} = \frac{u\Delta t}{\Delta x} \leq 1$). The Smagorinsky-Lilly subgrid-scale model was used to model the subgrid flow. It was found that the flow predicted using LES was realistic, showing the asymmetric flow and velocities in the same region as found experimentally.

Ni *et al.* then conducted a more in depth study on using LES to model OBC's (2003NI01). This was again compared to results from DPIV. Numerical simulations were run between Re_o = 156-2500, but phase averaged results are only reported for Re_o = 1250. An unstructured mesh with 406 136 cells was used. This was deemed to be fine enough by mesh independence studies. Although a finer mesh of 780 040 cells gave phase averaged velocity magnitudes and integral length scales closer to the experimental data, the turbulent kinetic energy was virtually the same for all the meshes used, showing that all the grids were fine enough to put the cut-off within the inertial sub-range, and therefore a coarser mesh was chosen to reduce computational expense. Again the Smagorinsky-Lilly subgrid-scale model was used. A time step of 0.0125s was used. There was a reasonably good correlation between LES results, and DPIV results, with the mean velocities, and cycle averaged turbulent kinetic energy from DPIV being higher, most likely because the velocities in the near-wall areas can't be resolved using DPIV. Like his previous study (2002NI01), Ni found that the sub-grid turbulent kinetic energy was small in magnitude, showing that the mixing is mainly due to the resolved velocities.

The latest study conducted in the numerical modelling of OBC's was by Chew *et al* (2004CH01). This was performed on an OBC of 30mm diameter, baffle spacing of

48mm, slightly larger than generally accepted length of 1.5 times the column diameter, and orifice diameter of 15mm, approximately 0.6 times the size of the OBC used by Ni (2000NI01, 2002NI01, 2003NI01, 2003FI01, 2003JI01). A grid with 443 520 cells was used, along with a time step of 0.0025s. Simulations were conducted at $Re_o = 5654$ ($x_0 =$ 3mm, $f =$ 10Hz), and $Re_o = 9425$ ($x_0 =$ 5mm, $f =$ 10Hz), and both the RNG k-ε turbulence model, and LES, with a RNG-based subgrid-scale model, were tried. The RNG k-ε model maintained an axisymmetric flow over 15 oscillations at $Re_o = 9425$, whereas the simulation using LES developed asymmetric flow after 7 cycles.

The asymmetric flow predicted using LES was more consistent with experimental observations by Mackley (2002MA01), and LES was therefore used for the rest of the simulations. The spatial and temporal shear rate distributions were calculated and compared to those of an impeller driven stirred vessel. It was found that particles in OBC's spent most of their time in areas of high shear rate.

3. Numerical Modelling Strategy

Computational Fluid Dynamics has relatively recently found widespread industrial application due to the rapid growth in computational speed and resources. It is performed by splitting the computational domain into finite volumes, and then solving the discretised form of the governing equations over the finite volumes.

Governing Equations

Conservation of Mass

The equation governing mass conservation, or continuity is as follows

$$div\mathbf{V} = 0 \tag{3.1}$$

Conservation of Momentum

Since the flow is time dependent, the basic governing equations used are the unsteady, incompressible Navier-Stokes equations, given by White (2001WH01)

$$\rho\frac{D\mathbf{V}}{Dt} = \rho\mathbf{g} - \nabla p + \mu\nabla^2\mathbf{V} \tag{3.2}$$

For virtually all the combinations of oscillation amplitudes and frequencies that are to be tested, the flow is in the turbulent regime. Since the fluctuations in the flow are of such a small scale and of such high frequency, it would be far too computationally expensive to simulate the flow directly, and so either Reynolds Averaged Navier Stokes (RANS) turbulence models are used or Large Eddy Simulation (LES) is used.

3.1 RANS Turbulence Models

The RANS equations are formed by decomposing the variables in the exact Navier Stokes equations into their average and fluctuating components

$$\phi_i = \bar{\phi}_i + \phi_i' \tag{3.3}$$

where ϕ_i is the instantaneous value, $\bar{\phi}_i$ is the average component and ϕ_i' is the fluctuating component. The Reynolds averaged equations are as follows (2001WH01).

$$\rho \frac{D\mathbf{V}}{Dt} + \rho \frac{\partial}{\partial x_j}\left(\overline{u_i' u_j'}\right) = \rho \mathbf{g} - \nabla \bar{p} + \mu \nabla^2 \overline{\mathbf{V}} \tag{3.4}$$

The turbulence models provide closure to these equations by modelling the so called Reynolds stresses $\rho \overline{u_i' u_j'}$.

3.1.1 k-ε Turbulence Model

One way of doing this is by using the Boussinesq hypothesis, shown in Eq. 3.5, which relates the Reynolds stress to the mean flow strain.

$$-\rho \overline{u_i' u_j'} = \mu_t \left(\frac{\partial u_i}{\partial u_j} + \frac{\partial u_j}{\partial x_i} \right) - \frac{2}{3}\left(\rho k + \mu_t \frac{\partial u_k}{\partial x_k} \right) \delta_{ij} \tag{3.5}$$

This is used in all one and two equation turbulence models, such as the Spalart-Allmaras, k-ε and k-ω models (1998WI01). This entails the Reynolds stress tensor being calculated as the product of the eddy viscosity and mean strain-rate tensor (1998WI01). This means that at all points in a turbulent flow, the principle axes of the Reynolds stress tensor are coincident with the axes of the mean strain-rate tensor (1998WI01), and that the turbulent viscosity is isotropic. This approximation makes these models computationally

inexpensive, but is not always true though, such as in flows with sudden changes in strain rate. Therefore flows where the dominating factor is anisotropy of turbulence cannot be modelled, such as stress-driven secondary flows (2004FL01*)* – exactly the type of flow found in the OBC. This means that one and two-equation models are unsuitable for modelling OBC's. This was also reported by Jian and Ni (2003JI01), who found that the RNG k-ε model predicted a flow that did not become asymmetric, as well as Chew (2004CH01), who also found the RNG k-ε model to maintain a symmetrical flow throughout the simulation.

3.1.2 Reynolds Stress Model (RSM)

The more complex second-order closure Reynolds Stress Model (RSM) instead solves the transport equation for the Reynolds stresses directly, as well as solving for the dissipation rate, abandoning the isotropic eddy viscosity assumption. By doing this the directional effects of the Reynolds stress field can be accounted for (1995VE01), and should therefore be able to model anisotropic flows. To do this, 7 additional transport equations need to be solved in 3D, making this model computationally expensive. The transport equations for the Reynolds stresses are shown in Appendix 1.

Although this turbulence model is able to predict the anisotropic flow that occurs in OBC's, it was found that simulations using LES, explained in Section 3.2, could also predict the flow with less computational expense. RSM was therefore not used for this research.

3.2 Large Eddy Simulation (LES)

LES is a relatively new alternative to RANS turbulence models. Filtered versions of the exact Navier Stokes are used as the governing equation. These are formed by separating velocity into its resolved and subgrid parts, as seen in Eq. 3.6

$$u_i(x,t) = \overline{u}(x,t) + u''(x,t) \tag{3.6}$$

By doing this the larger, energy containing eddies are directly resolved, and the smaller, subgrid dissipating eddies are modelled using an algebraic model. This is done since the larger energy-containing eddies are more dependent on the boundary conditions and therefore it's almost impossible to universally model them, unlike the subgrid eddies, which are more isotropic, making it easier to find a universal model that can accurately model them.

The filtered Navier Stokes equations are as follows:

$$\frac{\partial \overline{u}_i}{\partial x_i} = 0 \tag{3.7}$$

$$\frac{\partial}{\partial t}(\overline{u}_i) + \frac{\partial}{\partial x_i}(\overline{u}_i \overline{u}_j) = \frac{\partial}{\partial x_i}\left(\nu \frac{\partial \overline{u}_i}{\partial x_j}\right) - \frac{\partial \overline{p}}{\partial x_i} - \frac{\partial \tau_{ij}}{\partial x_j} \tag{3.8}$$

To model the subgrid scale turbulent stresses, the following equation is used

$$\tau_{ij} - \frac{1}{3}\tau_{kk}\delta_{ij} = -2\mu_t \overline{S}_{ij} \tag{3.9}$$

where

$$\overline{S}_{ij} = \frac{1}{2}\left(\frac{\partial \overline{u}_i}{\partial x_j} + \frac{\partial \overline{u}_j}{\partial x_i}\right) \tag{3.10}$$

To model μ_t, a subgrid-scale (SGS) model is used. All the SGS models use the Boussinesq eddy viscosity hypothesis. Two models were used in this work - the standard Smagorinsky-Lilly model, which is the most widely used and simplest subgrid model (2004FL01), and the dynamic Smagorinsky-Lilly model. The latter model was only available with FLUENT 6.2.16, and therefore wasn't available at the time of Ni *et al*'s

research (2002NI01, 2003JI01, 2003NI01), which used FLUENT 5. For this reason, all simulations were first conducted using the standard Smagorinsky-Lilly SGS model so that the model used by Ni *et al* (2002NI01, 2003JI01, 2003NI01) could be validated. These SGS models make the assumption that all the kinetic energy from the large, is not a universal constant resolved eddies is transferred to, and therefore dissipated into heat by the small, subgrid eddies, and therefore the subgrid eddies can be modelled by using the resolved velocity values.

The standard Smagorinsky-Lilly model is a simple algebraic model

$$\mu_t = \rho L_s^2 \left|\overline{S}\right| \tag{3.11}$$

where $\left|\overline{S}\right| \equiv \sqrt{2\overline{S_{ij}}\,\overline{S_{ij}}}$ and L_s is the mixing length and is defined by

$$L_s = \min(\kappa d,\ C_s V^{1/3}) \tag{3.12}$$

d is the distance to the closest wall, κ is the von Kármán constant, which equals 0.42, and C_s is the Smagorinsky constant, which was set to 0.1, since this value is most applicable to the widest range of flows according to the FLUENT users guide (2004FL01). One of the main drawbacks of the standard Smagorinsky-Lilly model is that C_s is not a universal constant, but varies according to the resolved flow, and this can result in inaccuracies in the flow predicted by this model, especially when modeling transitional flows.

The dynamic Smagorinsky-Lilly model dynamically calculates the value of C_s based on the resolved scales of motion, rather than using a fixed value of 0.1. This value varies between cells and changes with time, and therefore the dynamic model should be potentially more accurate than the standard Smagorinsky-Lilly model. FLUENT does however limit the values of C_s to a range between zero and 0.23 to avoid numerical instability. Unlike the Standard Smagorinsky-Lilly, the Dynamic model can accurately predict the transitional flow, as well as account for near-wall damping.

3.3 Time Step Size

The time step size used in this research was 0.005s, with second order implicit temporal discretization. This was 2.5 times as small as the time step used by Ni *et al* (2003JI01, 2003NI01) and double the time step used by Chew *et al* (2004CH01). This time step size gives a Courant-Friedrich-Levy (CFL) number ($N_{CFL} = \frac{u\Delta t}{\Delta x}$) equal to 1 in the majority of the flow, apart from very isolated areas where the grid is very fine and there is a large velocity magnitude. This value did not exceed 3 in any areas though.

3.4 Discretization Schemes

It is not mentioned in Ni's work which discretization schemes were used apart from the central differencing momentum discretization scheme (2003NI01). Therefore, for the initial simulations, all the default discretization schemes were used. FLUENT 6.2.16 automatically uses the Bounded Central-Differencing (BCD) momentum discretization scheme when LES is selected to overcome the sensitivity of LES to numerical diffusion. This is a composite scheme consisting of pure central differencing, a blended scheme of central differencing and 2nd order upwind, and 1st order upwind. The 1st order upwind scheme is only used when the convection boundedness condition (CBC) is violated though (2004FL01). The standard pressure discretization scheme and the SIMPLE pressure-velocity coupling discretization scheme, explained below, are also defaults and were therefore used for the initial simulations investigating the effects of different grid sizes. Other discretization schemes were then investigated once the most appropriate grid size was found. A brief description of the different discretization schemes that were investigated is given in the following sections.

3.4.1 Pressure-Velocity Coupling

For the pressure-velocity coupling scheme, apart from the default SIMPLE scheme, the two other schemes available, SIMPLEC and PISO were also investigated. PISO can maintain a stable solution when using a large time step, and therefore recommended for

transient flows, and also for highly distorted grids due to its skewness correction (2004FL01). However, since a fully structured grid was used, combined with the fact that LES needs small time steps anyway and PISO is computationally more expensive, it was thought that SIMPLEC would be the more appropriate scheme to use for this model. Simulations were conducted with both schemes to confirm this.

3.4.2 Momentum Discretization Scheme

Once the most appropriate pressure-velocity coupling scheme was chosen, the effect of the different momentum discretization schemes was then investigated. The effects of numerical diffusion can easily overcome the effects of subgrid modelling in LES, and therefore it is important to use a momentum discretization scheme that introduces minimal diffusion. As a result the upwind based schemes, as well as the power law scheme were not appropriate when using LES. Since the bounded central differencing scheme can revert to the 1st order upwind scheme if certain criteria are not satisfied, it was not used. The Central Differencing (CD) and QUICK momentum discretization schemes are compared in this study.

The CD scheme uses linear interpolation to calculate the cell face quantities, and by Taylor Expansion, it can be shown that it is 2nd order accurate when using a uniform grid (1995VE01). Since this scheme takes equally weighted values from both the nodes of the cells sharing the face, it does not have the quality of transportiveness, i.e. it doesn't take in to account the strength of influence of the flow direction. Because of this, unrealistic flow will be predicted when this scheme is used for high velocity flow if the grid is not adequately refined

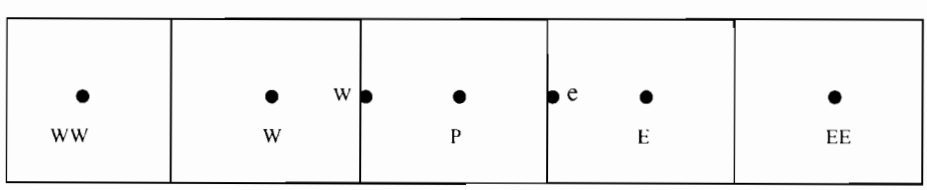

Figure 3-1. Uniform 2D grid

On a uniform grid as in Fig. 3-1, the face values of a property ϕ are calculated as follows when using the CD scheme

$$\phi_e = (\phi_P + \phi_E)/2 \tag{3.13}$$

$$\phi_w = (\phi_W + \phi_P)/2 \tag{3.14}$$

The QUICK (**Q**uadratic **U**pwind **I**nterpolation for **C**onvective **K**inetics) scheme on the other hand uses a three-point upstream-weighted quadratic interpolation (1995VE01). Weighted values from two upstream nodes and one down stream node are used to calculate the face value. Since two upstream nodes are used, the QUICK scheme is transportive.

On a uniform 2D grid as in Fig. 3-1 the following equations are used by the QUICK scheme to calculate the face values of a property ϕ

$$\phi_e = \frac{6}{8}\phi_P + \frac{3}{8}\phi_E - \frac{1}{8}\phi_W \tag{3.15}$$

$$\phi_w = \frac{6}{8}\phi_W + \frac{3}{8}\phi_P - \frac{1}{8}\phi_{WW} \tag{3.16}$$

By Taylor Expansion, it can be shown that the QUICK scheme is 3rd order accurate when using a uniform grid (1995VE01).

3.4.3 Pressure Discretization Scheme

Along with the Standard pressure discretization scheme, the PRESTO! (**PR**essure **ST**aggering **O**ption) discretization scheme was also investigated. Although the standard scheme works well if the pressure gradient between cells is small, it will predict inaccurate velocity values if there are large pressure gradients present (2004FL01). Therefore the scheme is inaccurate when used with highly swirling flows, flows with large body forces, or any other sources of high pressure gradient. The PRESTO! scheme

overcomes this by using a staggered grid to calculate the face pressures, and it is therefore thought that this scheme might show increased accuracy when simulating the flow near the baffles and in certain areas of high pressure gradients, such as around the large vortices.

3.5 Model Geometry

The geometry of the model used in this research is exactly the same as the model used in all OBC research conducted by Ni (2002NI01, 2003JI01, 2003NI01). All models were created in Gambit 2.2.30. Three baffled cells are modeled. The dimensions of the column model used for these simulations, as can be seen in Fig. 3-1, had a total length of 231mm, a pipe diameter of 50mm and distance between the baffles of 75mm. The baffles were 3mm thick and had an orifice diameter (D_o) of 23mm, giving a D/D_o value of 2.174. The distance between the baffles is 1.5 times the pipe diameter, which according to Brunold (1989BR01) is the spacing that gives the most mixing over the greatest range of amplitudes.

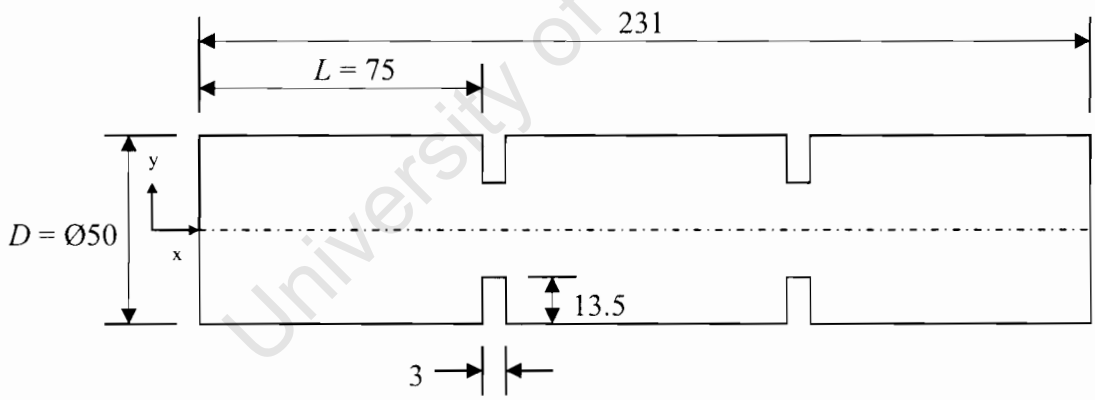

Figure 3-2. Dimensions of baffled column (All dimensions in mm)

The working fluid used was water (ρ = 998.2 kg m^{-3}, μ = 0.001003 kg m^{-1}s^{-1})

4. Computational Grid

A fully structured mesh was used for all the grids used in order to minimize numerical diffusion. Three different size grids were used to model the OBC. Grid 1 contained 551 225 cells, grid 2 contained 627 776 cells and grid 3 contained 726 804 cells. Consideration was taken to ensure that for all grids $y^+ = 1$ along the walls, although in very isolated points where there were high velocities near the walls, y^+ was as high as 5. Since this area of higher y^+ values moved throughout each cycle because of the oscillatory flow, a large area would have had to have been refined. Because of this, combined with the fact that the areas of high y^+ values were extremely isolated, it was decided that the meshes were adequate for use with LES.

The filter length used for LES is equal to the grid size. It is important to use a grid with a cell size that is between the size of the large energy absorbing eddies and the small dissipating eddies. This range of eddy sizes is called the inertial sub-range and there should be effectively neither generation, nor dissipation of turbulent kinetic energy in this size range. According to Schubert (1999SC01) eddies that have a radius smaller than 12 times the size of the Kolmogorov length scale (l_D), defined in Eq. 4.1, are laminar dissipating eddies.

$$l_D = \left(\upsilon^3/\varepsilon\right)^{1/4} \tag{4.1}$$

The grid size should also be in this range in order to be in the inertial sub-range. By calculating ε from the combination of the experimental values given by Ni (2003NI01), the average value is approximately $6\text{x}10^{-4}$ m^2/s^3. Since υ for water is 10^{-6} m^2/s, this means the average grid size should be approximately 2.42 mm. Since the flow is highly dynamic, there are areas in the flow however that reach values of ε into the region of $6\text{x}10^{-3}$ m^2/s^3, meaning a filter length of 1.36mm is needed in these areas. Both these grid sizes are very large, and it is thought that using a grid of this size would cause numerical inaccuracies, since y^+ and CFL numbers would be higher than 1. It was therefore

attempted to make the filter length in the region of 0.3mm in areas where it was thought that the dissipation rate would be highest, and use a coarser grid in other areas. If the grid is finer than the size of the laminar eddies, it means that more of the flow is directly resolved, and less is modeled, which should produce a more accurate result. Schubert's research (1999SC01) was based on impeller driven flotation cells though, so it was not known whether his findings could also be used for OBC's. Therefore simulations were still conducted to see whether the grid size was in the inertial sub-range. This was done by calculating the subgrid TKE, defined in Eq. 4.2, using the different grids.

$$k_{sgs} = \frac{\mu_t^{\,2}}{\rho^2 L_s^{\,2}} \tag{4.2}$$

If there was no change in the results using finer grids, then the grid size, and therefore the filter length could be deemed to be in the inertial subrange.

The mesh used in the inter-baffle cells on the ends of the model was coarser than the mesh used in the center cell, seen in Fig. 4-1. This was because results were only being compared in the center cell, and therefore it didn't matter if the flow simulated at the ends was accurate. The filter length in the side cells is under the filter length needed according to Schubert though. As mentioned before, Roberts (1996RO01) found that the flow in each cell was largely independent of the flow in the adjacent cells, and therefore it should not matter if the flow in these outer cells is not accurate. Another reason is that if a grid was used in the outer baffled cells of the same density as the center cell, the grid would be too large and computationally expensive. A typical grid is shown in Figs 4-1, 4-2 and 4-3.

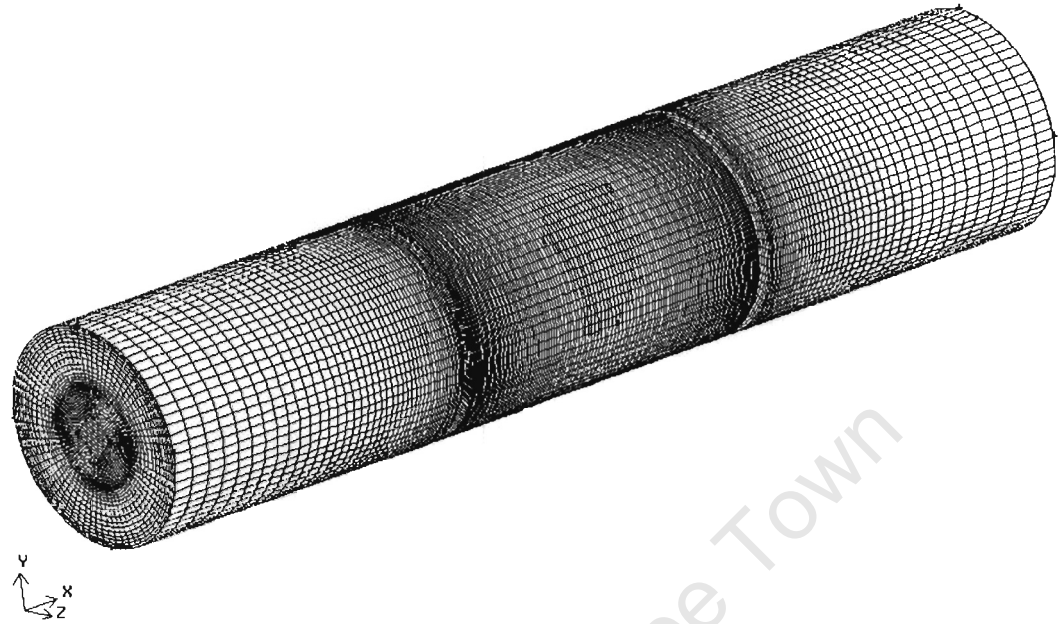

Figure 4-1. Typical OBC grid used

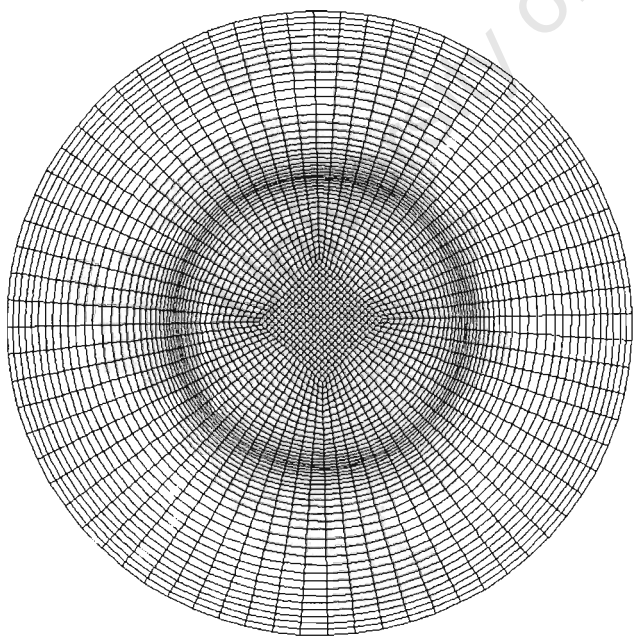

Figure 4-2. Typical axial cross-section of mesh through center-baffled cell

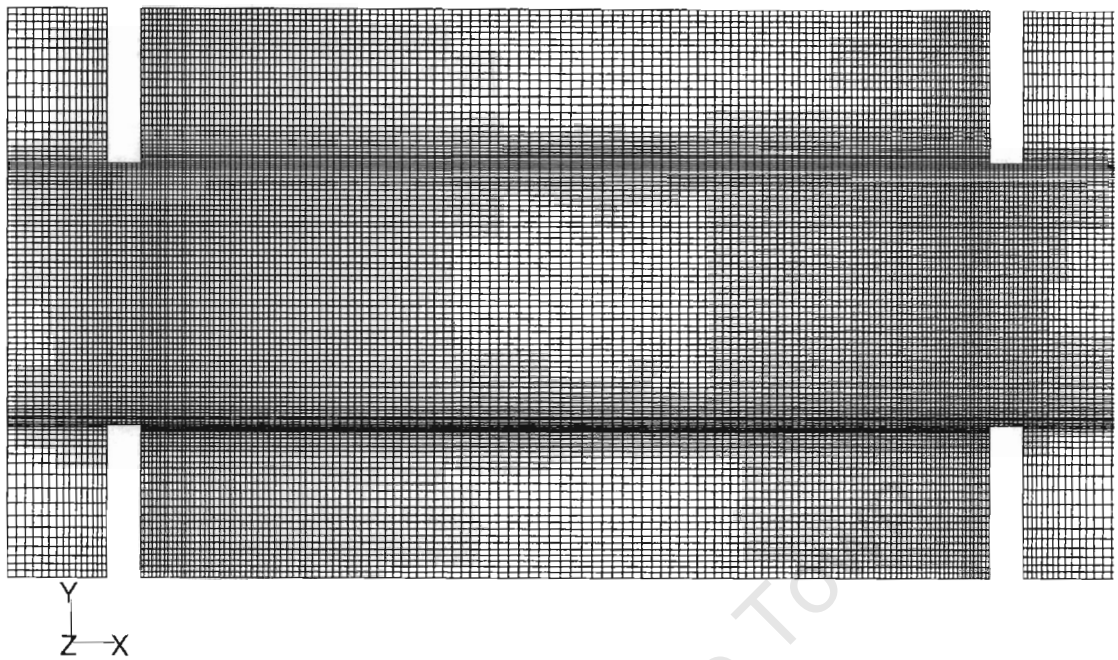

Figure 4-3. Typical longitudinal cross-section of grid in center baffled cell

5. Boundary Conditions

In all previous research, periodic boundary conditions have been used, whereby the flow through both ends of the OBC is forced to be both spatially and periodically identical. Since FLUENT does not allow periodic boundary conditions with transient flows, the mass flow rate had to be discretised and reset at each time step using a journal file. Since using periodic boundaries increases the computational expense of the simulation, velocity inlet boundary conditions were first investigated.

5.1 Velocity Inlet Boundary Conditions

Initially the oscillatory flow was defined by defining the one end of the OBC as a velocity inlet and the other an outflow. Effectively this would be the same as if a solid piston was on the left of the column, oscillating the flow. The flow at the velocity inlet was defined by a user defined function (UDF), which reset the velocity after each time-step through the OBC using Eq. 5.1:

$$u = 2\pi f x_o \cos(2\pi f t) \tag{5.1}$$

When the flow reversed, there would be reversed flow through the outflow boundary. The turbulent inlet conditions could be defined through the velocity inlet, but these values are usually found experimentally, and would therefore be difficult to estimate accurately. This method had the advantage that it would be less computationally expensive than using periodic boundaries, and according to Roberts (1996RO01), the flow in each inter-baffle cell is largely independent on the flow in the adjacent cells, and therefore it should not matter that the incoming flow into the side cells is not realistic, as it should develop in these before coming into the center cell.

5.2 Periodic Boundary Conditions

Translational periodic boundaries were also used. This is equivalent to the one periodic boundary having the opposing periodic boundary as its direct neighbor, thereby making the two boundaries have identical flow conditions. To define the oscillatory flow, a journal file (Appendix 2) was used that reset the mass flow rate through the boundaries at each time step using Eq. 5.2

$$\dot{m} = \rho\left(\frac{\pi}{4}D^2\right)2\pi f x_o \cos(2\pi f t) \tag{5.2}$$

Since the incoming flow is identical to the outgoing flow, the turbulent conditions will have already developed. Using periodic boundaries would be more computationally expensive because of the iterative procedure to get the flow though the boundaries to be identical, but the flow in reality is periodic and so this method is more realistic and therefore should give the most accurate results.

Simulations were also conducted to see the effect of using periodic boundaries that were the same diameter as the orifice, instead of them being the entire column diameter. This was done with the thought that it would produce a more realistic flow.

6. Data Used to Validate Model

All the DPIV experimental and numerical data used to validate the model was from work by Ni (2003NI01) where an oscillation frequency and amplitude of 1Hz and 4mm was used throughout. The DPIV data was in the form of phase averaged variable values averaged over one baffled cell. Due to the nature of the DPIV equipment, the area closer than 3mm to the walls of the OBC was not included in this average. Since DPIV can only provide two-dimensional measurements, the three dimensional velocity components were approximated as a ratio of the 2D components. It was chosen to compare the results against the 3D volume averaged results since the 2D results would change depending on the angle of the plane that they were taken on because of the asymmetric nature of the flow. These were averaged over 15 cycles. One of the problems with using volume averaged experimental results to validate the numerical model against is that vastly different flows could potentially produce the same volume averaged result. This therefore needs to be kept in mind when comparing results.

Each cycle was split into 8 phases as can be seen in Fig. 6-1. Values of velocity, turbulent kinetic energy, dissipation rate and integral length scale, defined in Sections 6.1, 6.2 and 6.3 respectively, were calculated at each of these phases, and then the volume weighted average was calculated over the cycles completed. This was done by exporting the cell velocity magnitudes at each phase and then using those data sets to calculate the resolved TKE, which is defined in Eq. 6.3, using an externally written FORTRAN program (Appendix 3).

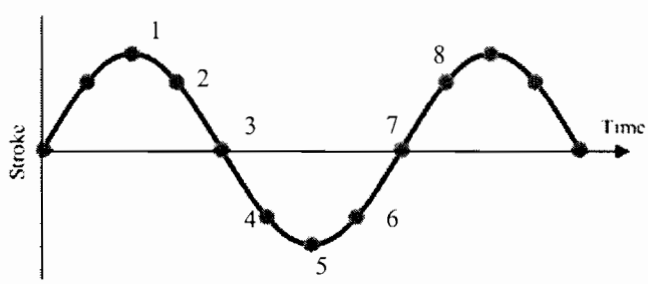

Figure 6-1. Phase positions with respect to time

Data was only begun to be recorded after 10 cycles to allow the flow to stabilize. Although the velocity components at different points in the flow were not constant at each phase at this point, the volume weighted velocity average was, and it was known that it could take over 100 cycles for the flow to reach a fully saturated asymmetric state (1996RO01). Therefore this was deemed a suitable point at which to begin to sample data. Values were then recorded for 4 cycles when the results were used for the comparison of different grids and discretization schemes as this was thought to be long enough since only their effect on the results was of interest, and not the actual result.

6.1 Turbulent Kinetic Energy (*k*)

Turbulent kinetic energy (TKE) is obtained by the summation of the subgrid TKE and resolved TKE. The subgrid TKE is directly calculated in FLUENT using Eq. 6.1

$$k_{sgs} = \frac{\mu_t^{\,2}}{\rho^2 L_s^{\,2}} \tag{6.1}$$

with $L_s = \min(\kappa d,\ C_s V^{1/3})$. Although C_s changes from cell to cell when using the Dynamic Smagorinsky-Lilly subgrid-scale model, a set value of 0.1 was used when calculating the subgrid TKE since the actual value of C_s at each cell was not available for calculations.

The resolved TKE is calculated by using the definition of TKE per unit mass

$$k = \frac{1}{2}\sum_{i=1}^{3} u_i' u_i' \tag{6.2}$$

where u_i' is the fluctuating part of the velocity. Since this cannot be directly calculated by FLUENT and that $u_i' = u_i - u_m$ where u_m is the phase averaged velocity, Eq. 6.3 was used instead

$$k = \frac{1}{2}\left[\frac{\sum_{i=1}^{N} u_i u_i}{N} - (u_m)^2\right] \tag{6.3}$$

Since FLUENT does not calculate the phase averaged velocity, it was necessary to export a data file of velocity in each cell at each phase and then use an externally written program to calculate the phase average velocity and thus the resolved TKE (Appendix 2).

6.2 Dissipation Rate (ε)

It is assumed that all the TKE that is transferred from the resolved eddies to the subgrid eddies is dissipated by the subgrid eddies. The rate of energy dissipation is calculated by using the resolved velocity field in the form of the strain rate tensor, the subgrid turbulent viscosity, which again is calculated using the resolved velocity field, and the fluid density.

$$\varepsilon = \frac{\mu_t}{\rho}\left|\bar{S}\right|^2 \tag{6.4}$$

Therefore by combining Eq. 6.4, Eq. 3.11 and Eq. 3.12

$$\varepsilon = C_s^{\,2} V^{2/3}\left|\bar{S}\right|^3 \tag{6.5}$$

Although only values of TKE and turbulent integral length scale were available in the literature (2003NI01), Ni's experimental and numerical energy dissipation rates could be calculated for comparison since the turbulent integral length scale is defined by Eq. 6.6

$$l = \frac{k^{3\ 2}}{\varepsilon} \tag{6.6}$$

The turbulent integral length scale is the distance of fluid elements moved due to turbulent eddies (2003NI01) and is usually used to describe momentum transport. This means that the larger the length is, the more intense the mixing is.

7. Results and Discussion

Initially all simulations using LES were conducted using the standard Smagorinsky-Lilly SGS model, and as mentioned before, the default discretization schemes were used at first. The two different methods of defining the oscillatory flow were first compared

Figure 7-1. Iso-surface of vorticity magnitude (68 s^{-1}), colored by velocity magnitude after 10 cycles, showing asymmetry of flow (f = 1Hz, x_o = 4mm)

7.1 Velocity Inlet versus Periodic Boundary Conditions

Simulations conducted using velocity inlet boundary conditions gave phase averaged velocity magnitudes that were far lower than the experimental, as can be seen in Fig. 7.2a, and results of subgrid turbulent kinetic energy and dissipation rate were also lower than the results obtained using periodic boundaries (cf. Figs. 7-2b and c). It is thought that this is because the flow that entered the computational domain was effectively laminar and uniform over the entire inlet, unrealistic in both cases, and the turbulent flow

did not have time to develop. It was attempted to estimate the turbulence intensity coming into the domain but this did not help since the amount to specify was not known, and in reality would have a varying profile, and therefore was not accurate.

The results predicted when using a velocity inlet do follow the same trends as the periodic boundary results however, and it is thought that using this method would be more accurate if an extra baffled cell was added to either side of the computational domain to give the flow more time to develop, but that would result in a larger grid, and due to the extra computational expense and lack of time, this could not be done.

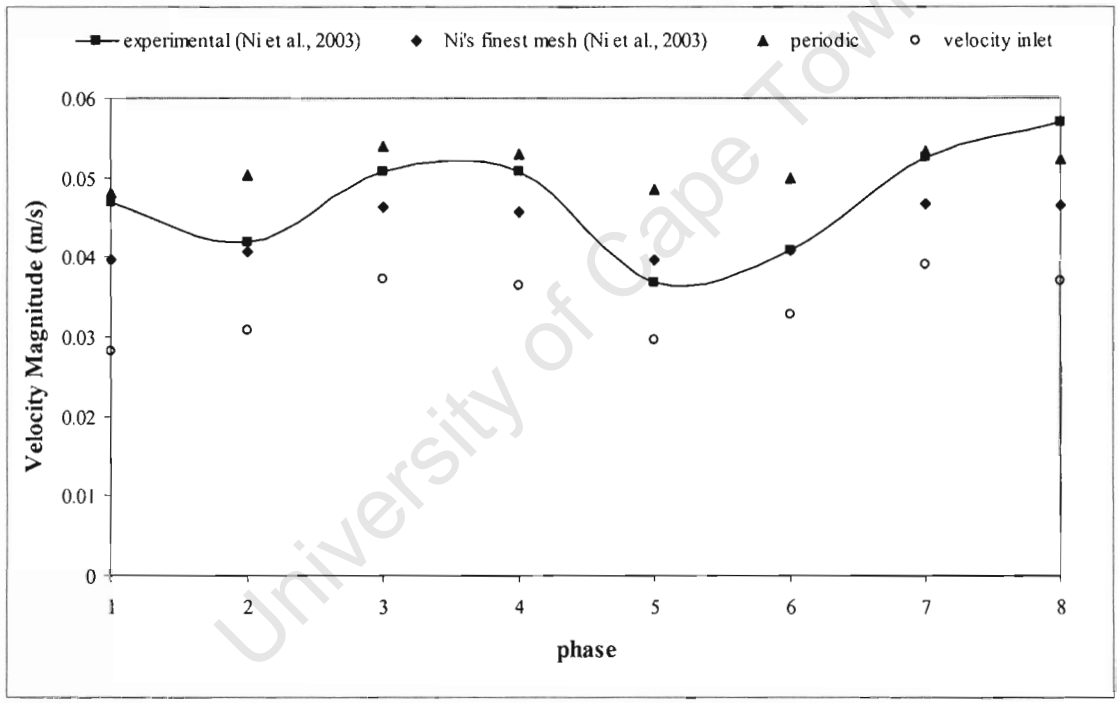

(a)

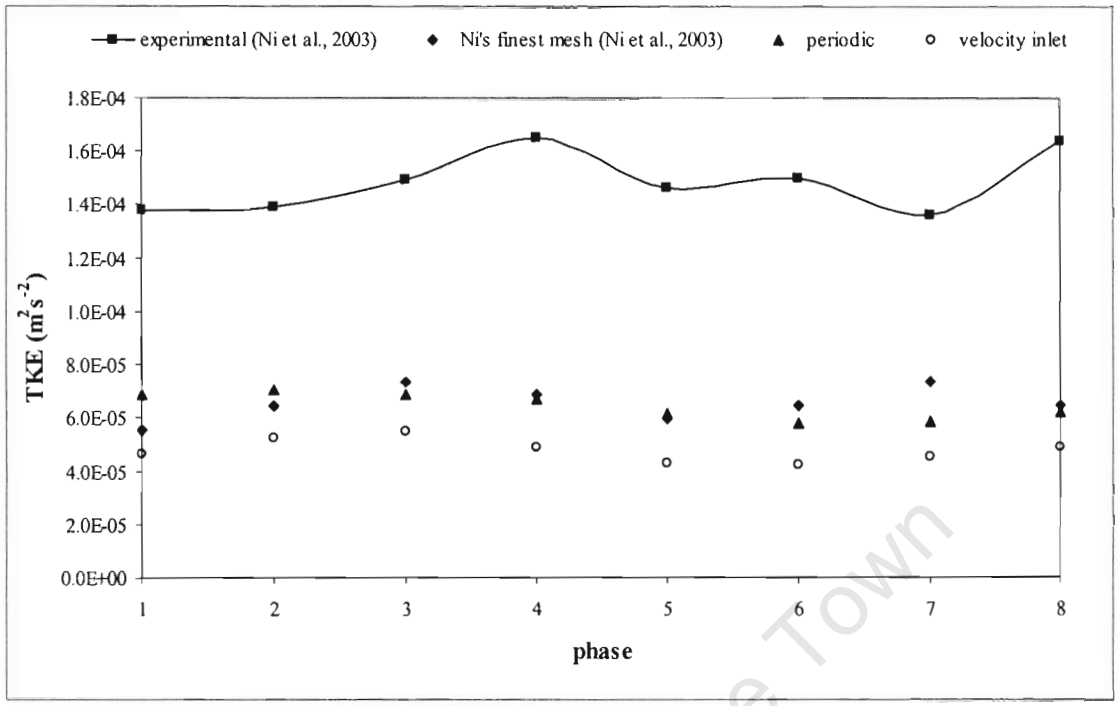

(b)

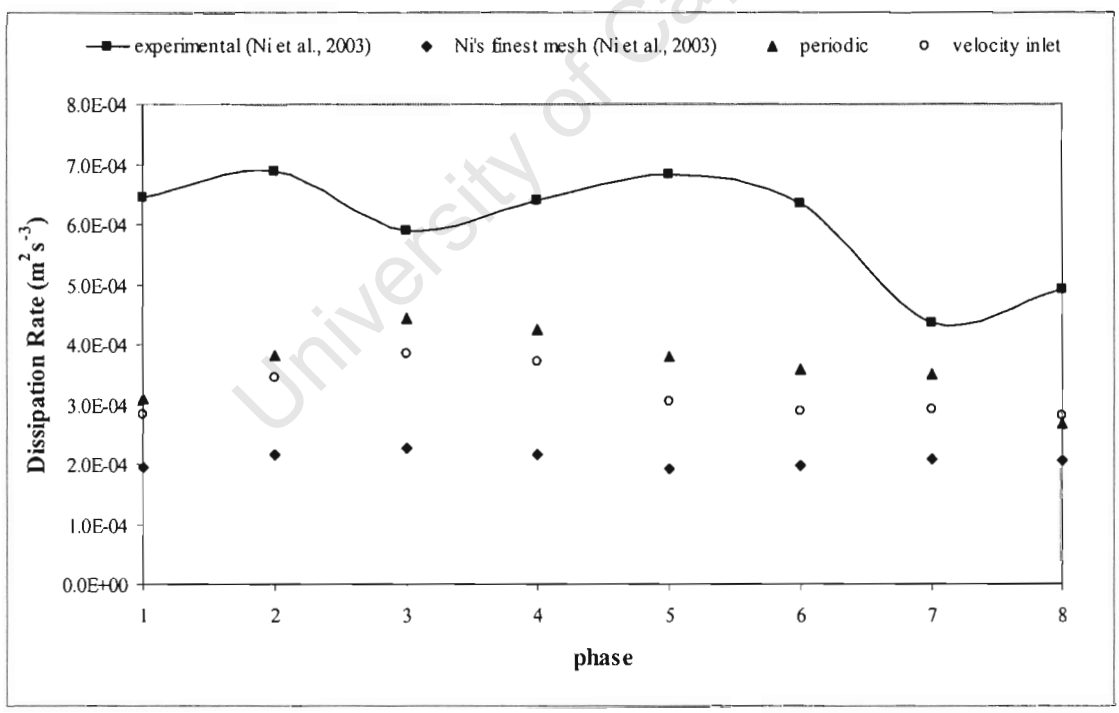

(c)

Figure 7-2. Comparison of the effects of using different methods of defining oscillating flow on phase averaged (a) velocity magnitude, (b) turbulent kinetic energy and (c) dissipation rate (f = 1Hz, x_o = 4mm)

Initial simulations using periodic boundaries gave results that were closer to the experimental results as can be seen in figs. 7.2a, b and c. The way the flow is defined using periodic boundaries is also more realistic, and therefore this method was decided to be used in subsequent simulations.

It was also attempted to use periodic boundaries that were only the orifice diameter, making the boundary conditions more realistic, but it was unable to reduce the residuals to less than $1x10^{-3}$. It is thought that the flow at each boundary was too different for the periodic boundary condition to force them to be the same, since at the one end of the column the flow would be suddenly expanding, and at the other end, contracting.

7.2 Convergence Independence

After conducting an initial simulation using grid 3 and the default discretization schemes, and using convergence criteria of $1x10^{-5}$ for the normalized residuals of continuity, x, y and z velocity, and momentum, the pressure gradient between the periodic boundaries was monitored. There was found to be no change in the gradient once residuals had been reduced to $5x10^{-4}$. Therefore for all subsequent simulations, the convergence criteria for all residuals were set to $5x10^{-4}$.

7.3 Grid Size Independence

It was found that there was minimal difference in the phase averaged velocity magnitudes between the results from the 3 different grids used, as can be seen in Fig. 7.3a. There was a small increase in TKE between grid 2 and 3 (cf. Fig. 7-3b), with the finer grid producing more accurate results, but little difference in TKE was predicted between results from grid 1 and 2. The same was found when comparing phase averaged dissipation rate, as is shown in Fig. 7-3c, except that there is clear improvement in the results when using grid 3.

The difference in the subgrid turbulent kinetic energy between the different grids was small, combined with the fact that there was no order in the results, i.e. grid 2 gave the

lowest subgrid TKE, with grid 3 giving the highest values (Fig. 7-3d). This points towards the conclusion that the subgrid TKE was no longer affected by the grid size, meaning that the filter length was in the inertial sub-range. This could also mean that the mesh that was used for grid 2 was not refined enough in place of high velocity. Because of the difference found between the results of subgrid and total TKE, as well as dissipation rate between grid 3 and the other two, it was decided that both simulations using grid 1 and 2 were grid dependent and therefore the most accurate grid to use would be grid 3.

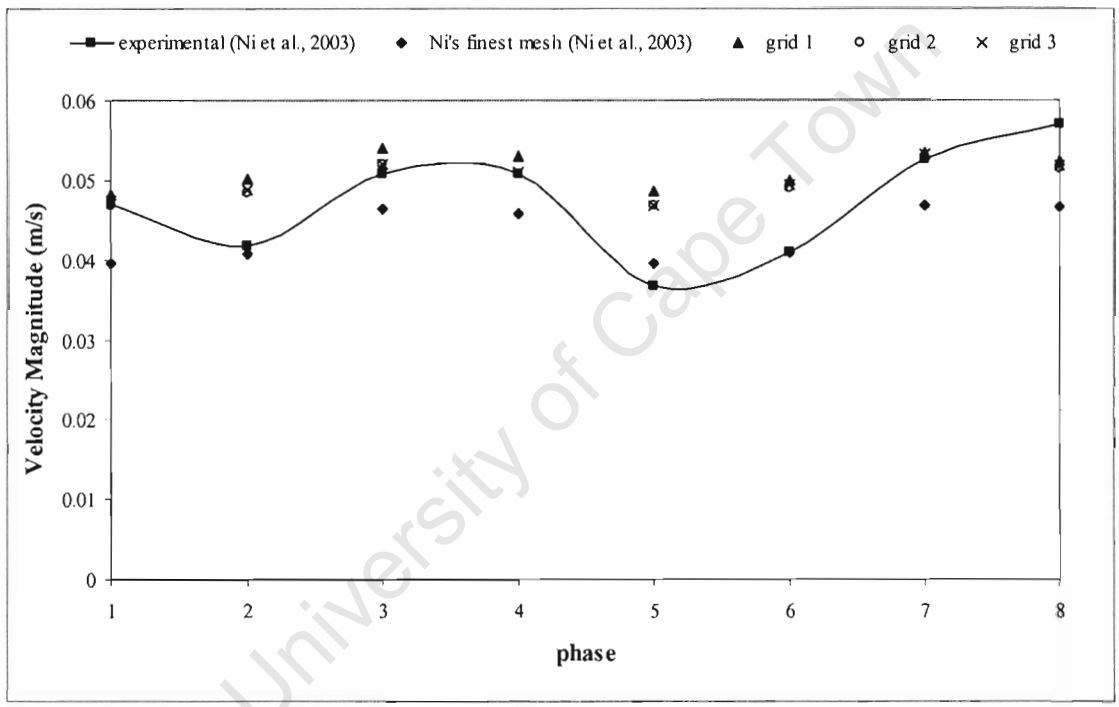

(a)

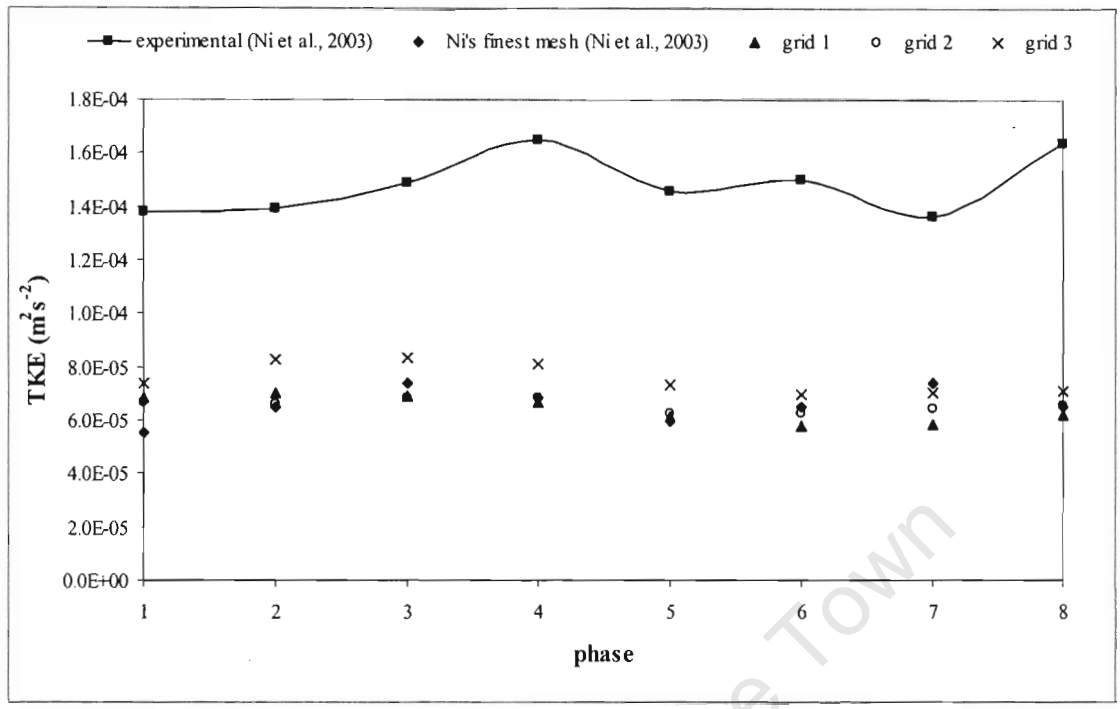

(b)

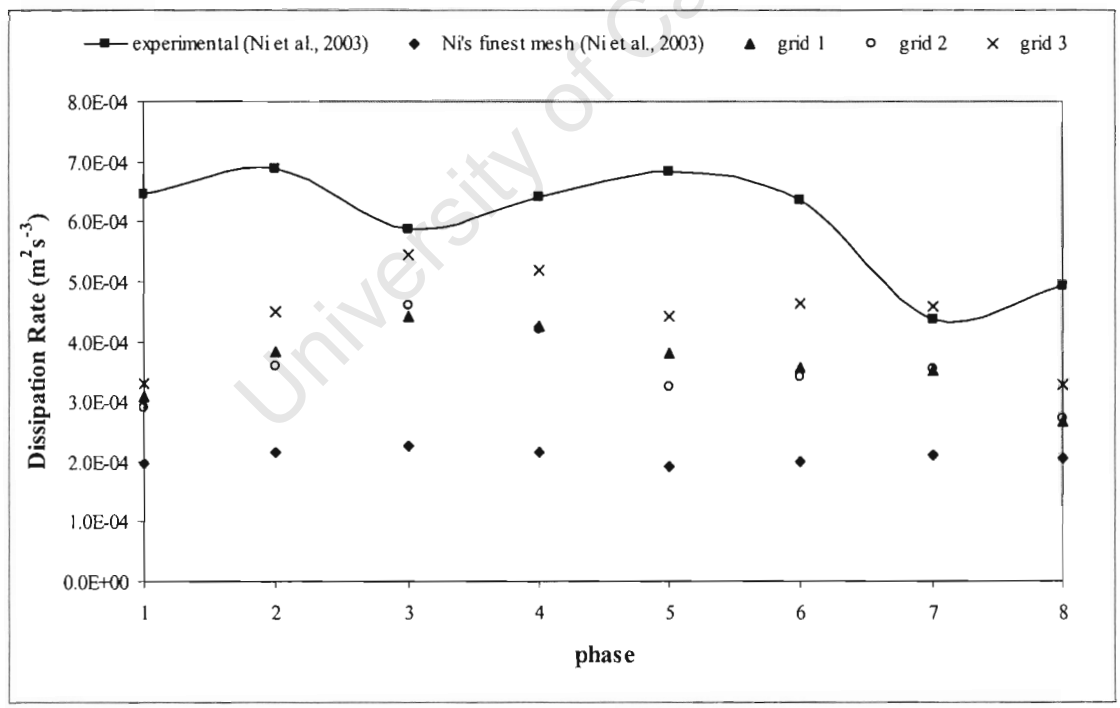

(c)

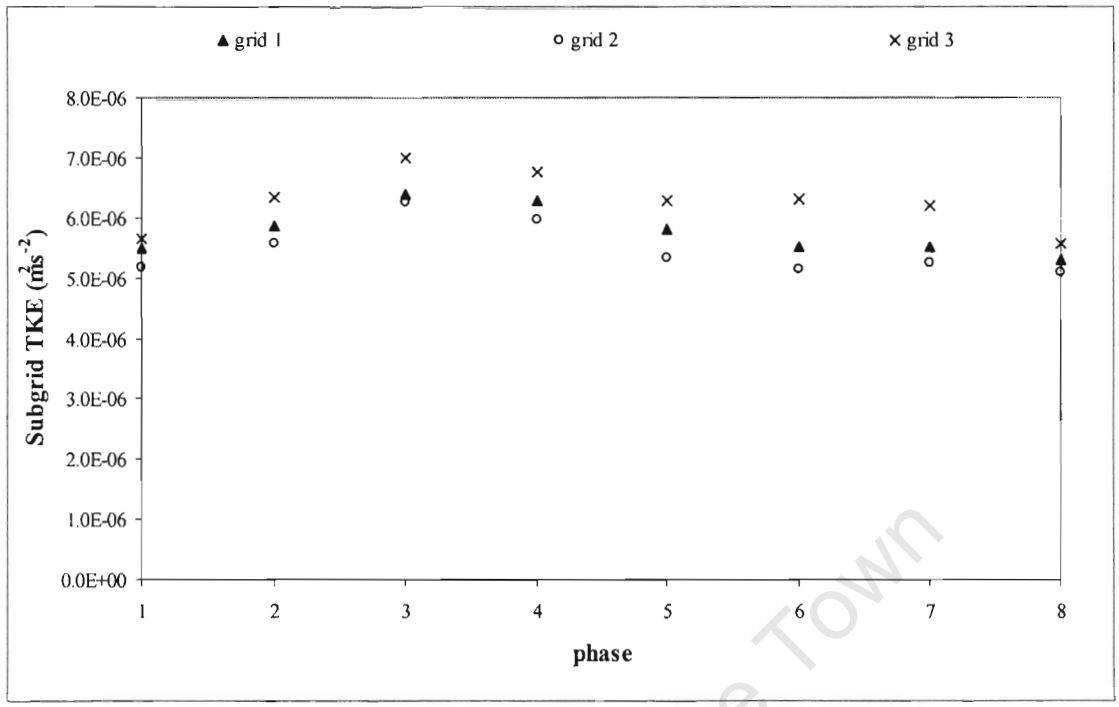

(d)

Figure 7-3. Grid effect on phase averaged values of (a) velocity magnitude, (b) integral length scale, (c) turbulent kinetic energy, and (d) the subgrid turbulent kinetic energy (f = 1Hz, x_o = 4mm)

7.4 Subgrid-scale (SGS) Models

Once the most appropriate grid was chosen, a simulation using the dynamic Smagorinsky–Lilly model was then conducted together with grid 1, and the default discretization schemes to investigate the effects of the subgrid scale models. Although this was not the most accurate grid to use, only the effect of the different SGS models was being investigated, and since the filter length of all the grids was in the inertial sub-range, there was therefore no need to use the finer grid that was more computationally expensive.

It was found that there was minimal change in the mean phase averaged results between the two subgrid scale models (cf. Fig. 7.4). Although the Standard Smagornisky-Lilly SGS model is less computationally expensive, it also has difficulty in predicting transitional flow (2004FL01). Because of the potential improvement in accuracy,

especially when this numerical model is used at higher Re_o numbers, it was therefore decided to use the Dynamic Smagorinsky-Lilly model for all further simulations.

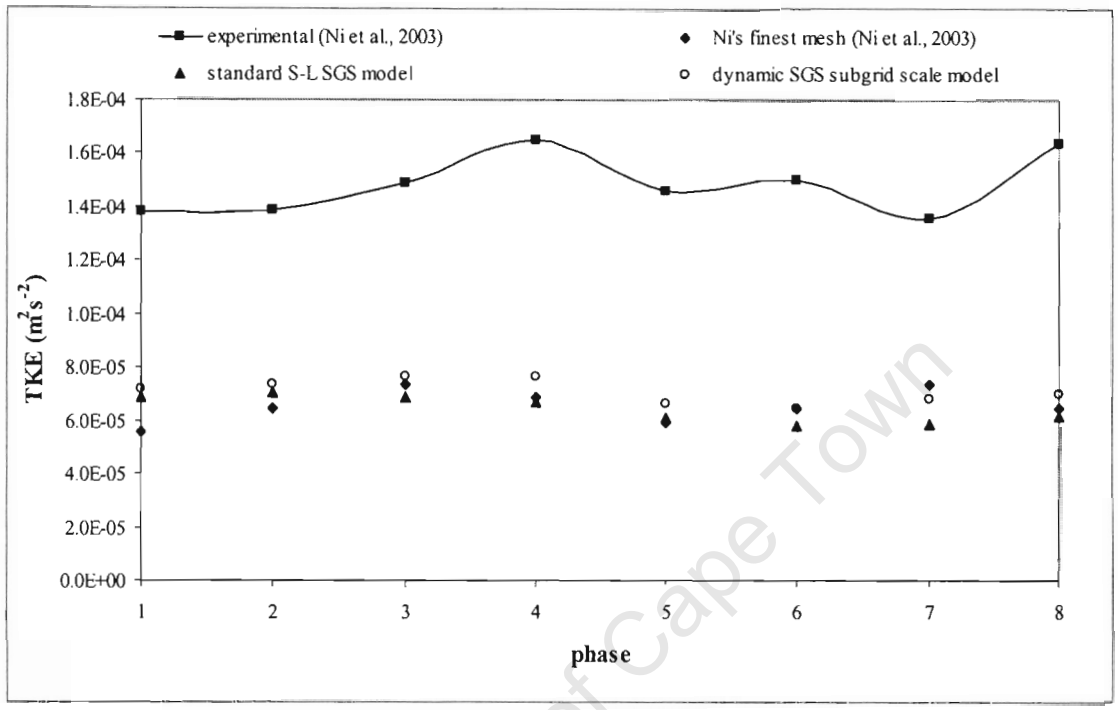

Figure 7-4. Effect of Dynamic Smagorinsky-Lilly subgrid-scale model on phase averaged results of turbulent kinetic energy (f = 1Hz, x_o = 4mm)

7.5 Discretization Schemes

7.5.1 Pressure-Velocity Coupling Discretization Scheme

Again using grid 1, since only the effect of the discretization scheme was being investigated, simulations were run using the dynamic Smagorinsky-Lilly SGS to investigate the effects of using different pressure-velocity discretization schemes. It was found that all pressure-velocity coupling schemes gave approximately the same results of phase averaged velocity magnitude and dissipation rate (cf. Figs. 7-5b and c). The SIMPLEC and PISO schemes predicted results of TKE that were on average slightly closer to experimental results than the SIMPLE scheme (cf. Fig. 7-5a). There was no significant difference between the SIMPLEC and PISO schemes. Due to this it was therefore decided that the SIMPLEC pressure-velocity discretization scheme was the

most appropriate scheme to use, along with the fact that it's less computationally expensive, confirming the initial notion stated in Section 3.4.1.

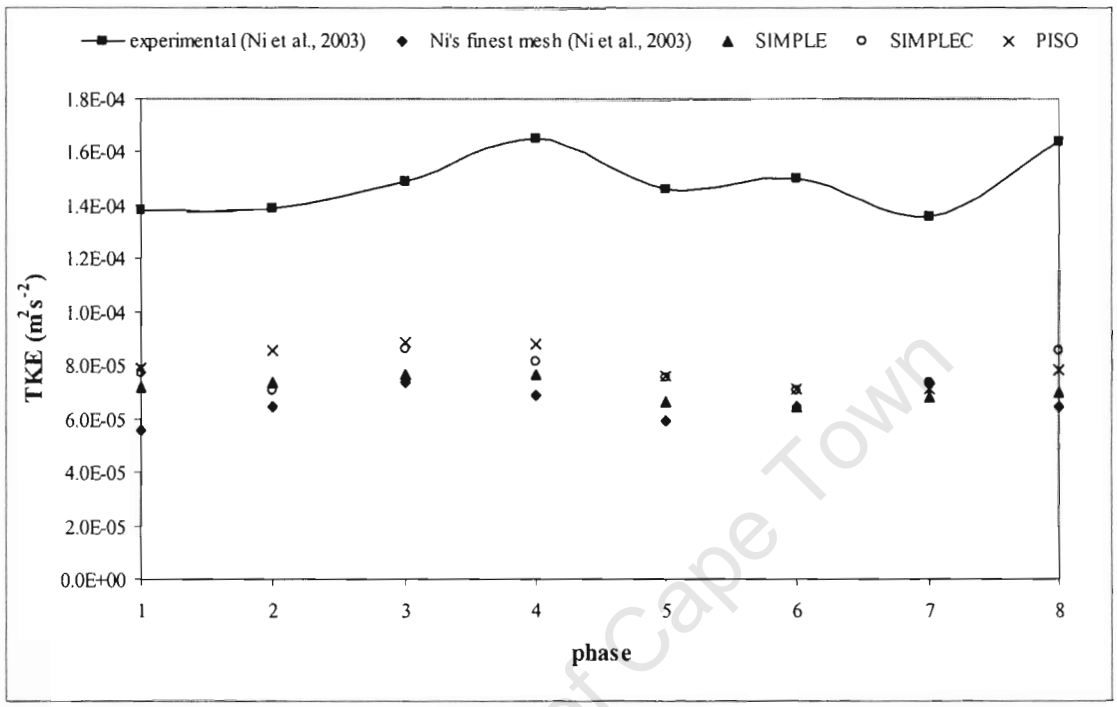

(a)

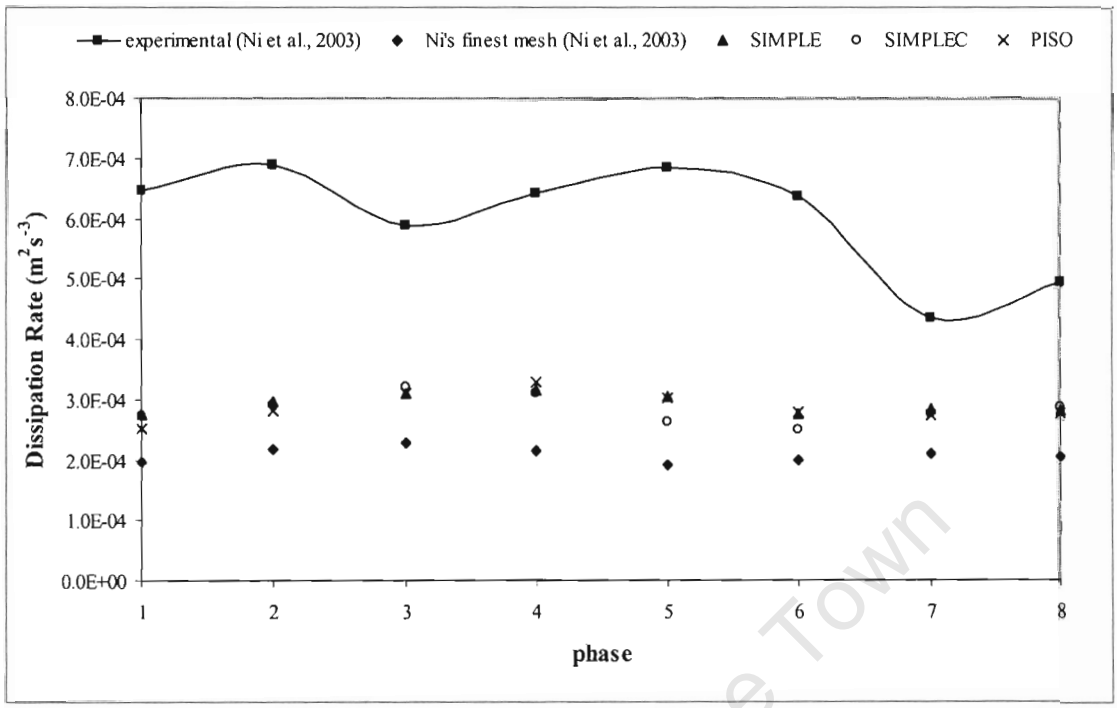

(b)

Figure 7-5. Effect of different pressure-velocity coupling discretization schemes on phase averaged results of (a) turbulent kinetic energy and (b) dissipation rate ($f = 1Hz$, $x_o = 4mm$)

7.5.2 Momentum Discretization Schemes

Using the SIMPLEC pressure-velocity coupling and the dynamic Smagorinsky-Lilly subgrid scale model together with grid 1, the CD and QUICK momentum discretization schemes were then compared. By observing the predicted flow, the first thing noticed was that the flow in the simulation using QUICK remained symmetric for a longer period of time than the flow when using CD, as is seen in Fig. 8-6a and b. Although the exact time of the flow becoming asymmetric was not established, the flow after 5 cycles was clearly symmetric when using QUICK, whereas the flow simulated using the CD scheme was already asymmetric at this point.

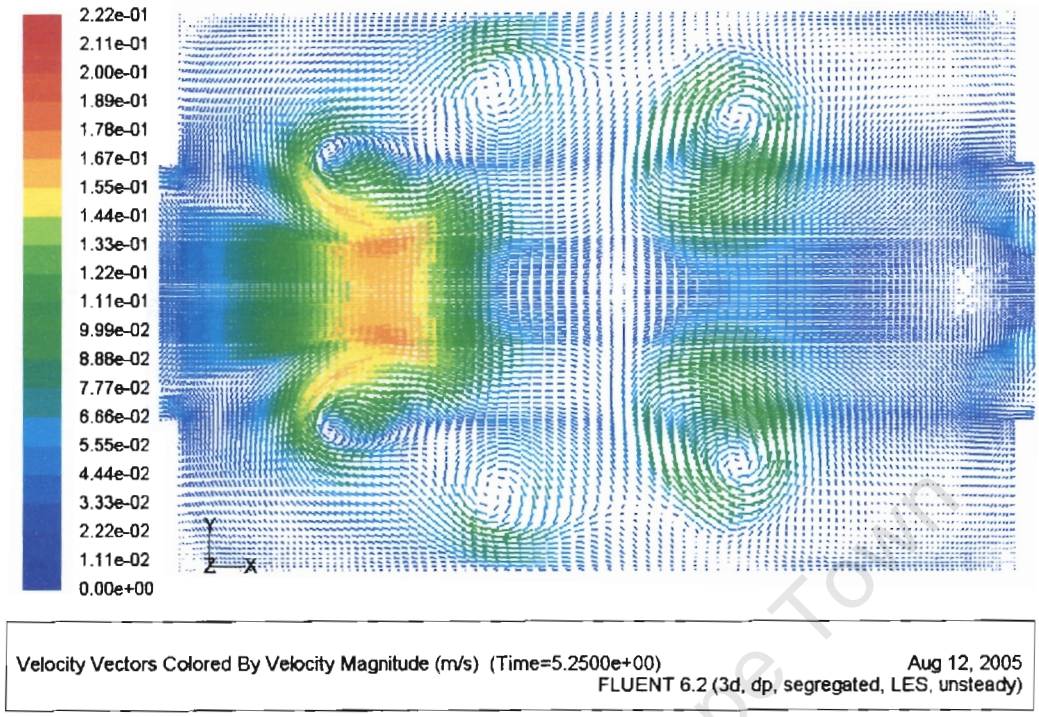

(a)

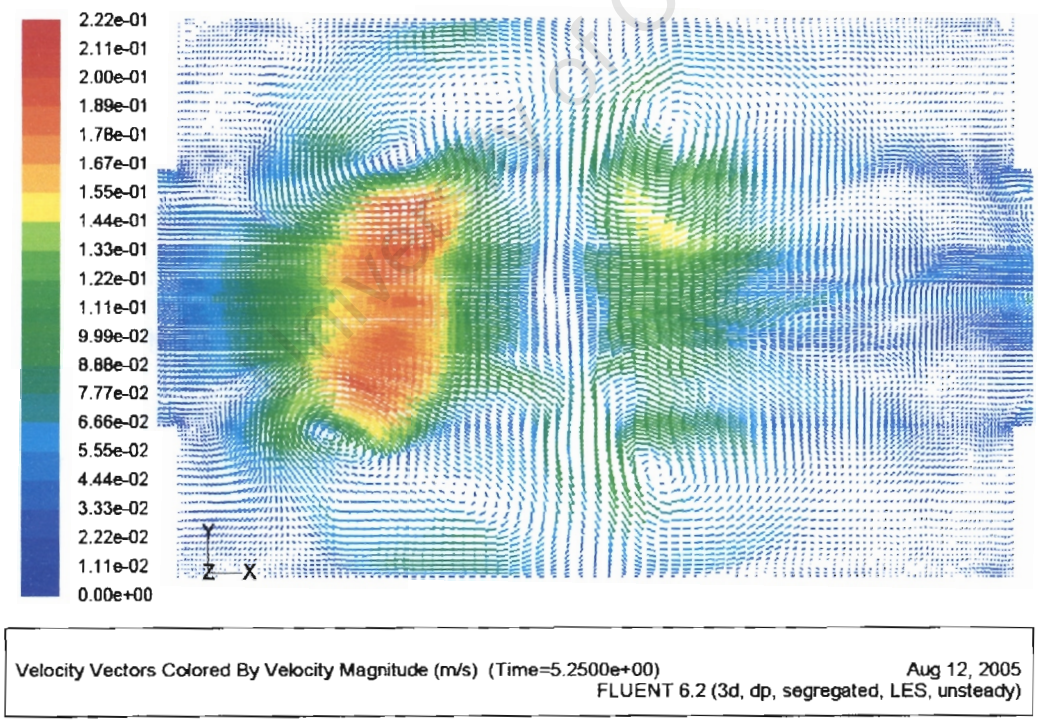

(b)

Figure 7-6. Velocity vectors at phase 1 after 5 cycles using (a) QUICK and (b) Central Differencing discretization schemes (f = 1Hz, x_o = 4mm)

The flow patterns after 10 cycles are also different, as is seen in Figs. 7-7a and b. Although both schemes show the same dominating eddies, the CD scheme predicts a highly asymmetric flow compared to the flow when using QUICK, which although asymmetric, is not asymmetric to the same degree.

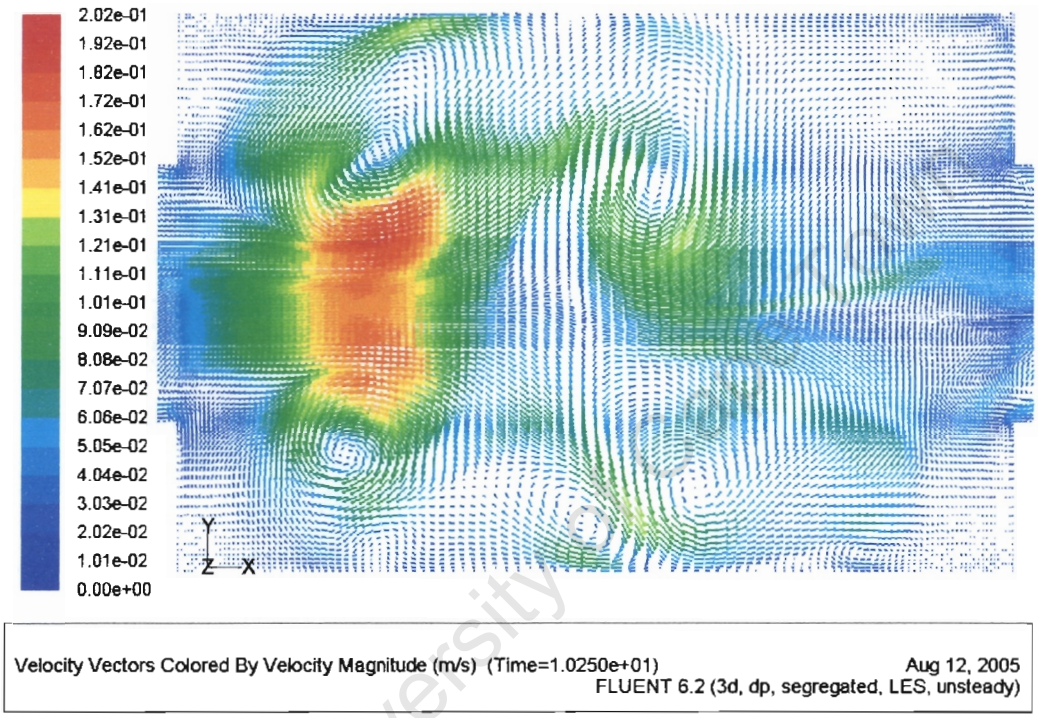

(a)

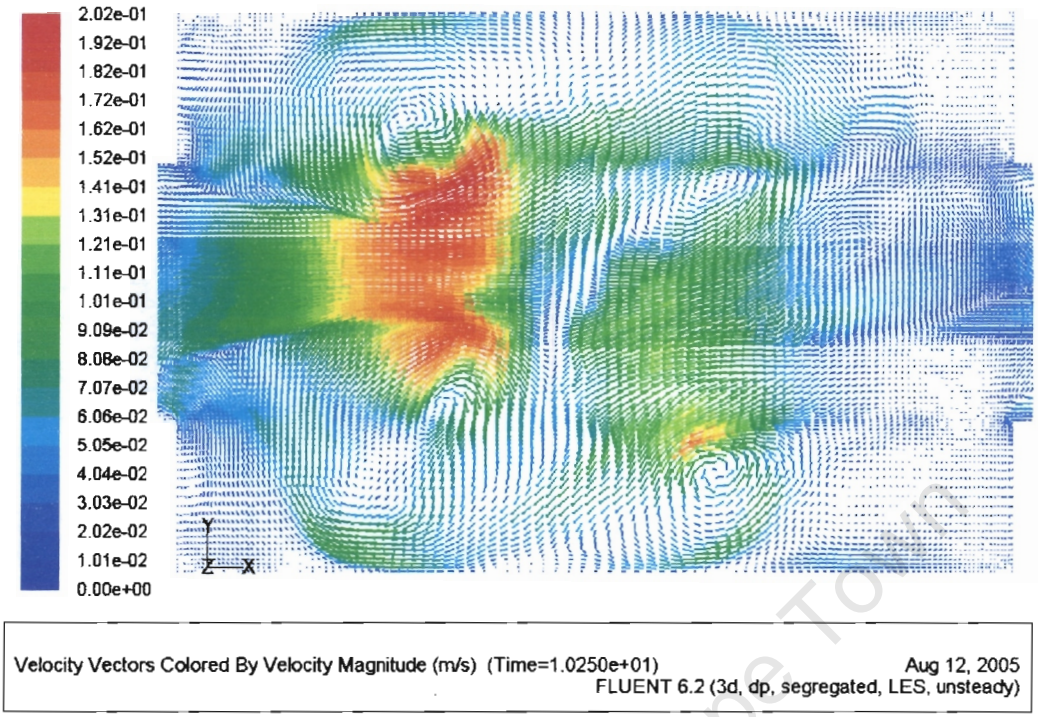

(b)

Figure 7-7. Velocity vectors at phase 1 after 10 cycles using (a) QUICK and (b) Central Differencing discretization schemes (f = 1Hz, x_o = 4mm)

It is thought that the early change and the high degree of asymmetry of the flow simulated using the CD scheme can be attributed in part to the tendency of the CD scheme to produce unrealistic permutations in the flow in areas of high velocity if the grid is not refined enough (1995VE01). Since each time-step uses the simulated flow from the last time-step as its initial condition, the permutations could cause an initial instability in the flow, and as the flow advances, this instability could permeate through subsequent time steps, making the flow become asymmetric earlier than in reality.

Although there is no mention in the literature of how many cycles it takes for the flow to become asymmetric experimentally at Re_o = 1250, St = 0.995, Chew *et al.* (2004CH01) observed that LES simulations run at Re_o = 5628, St = 0.796 became asymmetric after 13 cycles. Roberts and Mackley (1996) found that the development of asymmetry is dependent on the Oscillatory Reynolds number, so therefore it is assumed that the flow in

these simulations will become asymmetric in the region of 13 cycles, since they have a lower Re_o number.

Results of phase averaged mean velocity magnitude and TKE predicted using the CD and QUICK schemes were approximately equal, as can be seen in Fig. 7-8a.The fact that there was virtually no difference in results of mean velocity magnitude even though there was large difference in the predicted flows, as was seen in Figs. 7-6 and 7-7 indicates the inadequacies of volume averaged results when used to compare flows. Massively different flows could theoretically produce equal volume averaged results.

The CD scheme predicted results of phase averaged energy dissipation rate about 90% higher than the QUICK scheme, shown in Fig.7-8b. By looking at the equation for dissipation rate (cf. Eq. 6.5) the variables that affect dissipation rate are C_s and $|S|^3$. C_s only varies between 0 and 0.23 when using the Dynamic Smagorinsky-Lilly SGS model and could not be responsible for the significant differences. Therefore the strain rate is mostly responsible for the differences in the energy dissipation rate between the momentum discretization schemes.

Since $|S|$ is cubed, small differences could result in large differences in dissipation rate. Looking at the strain rate (Fig. 7-8c), it can be seen that the CD scheme does predict a slightly higher phase averaged strain rate. Therefore, although the CD scheme predicted a flow with dissipation rates that were closer to experimental results, this difference is only due to a small difference in strain rate. Due to the DPIV data not including the area 3mm from the walls in the averaging, which is the area of highest strain rate, it is not even certain if the experimental energy dissipation rate is accurate. Since the CD scheme predicted a premature change in the flow to the asymmetric regime, together with the fact that the QUICK scheme is a higher order scheme, and therefore numerically more accurate, it was therefore decided to use the QUICK scheme in all subsequent simulations.

.

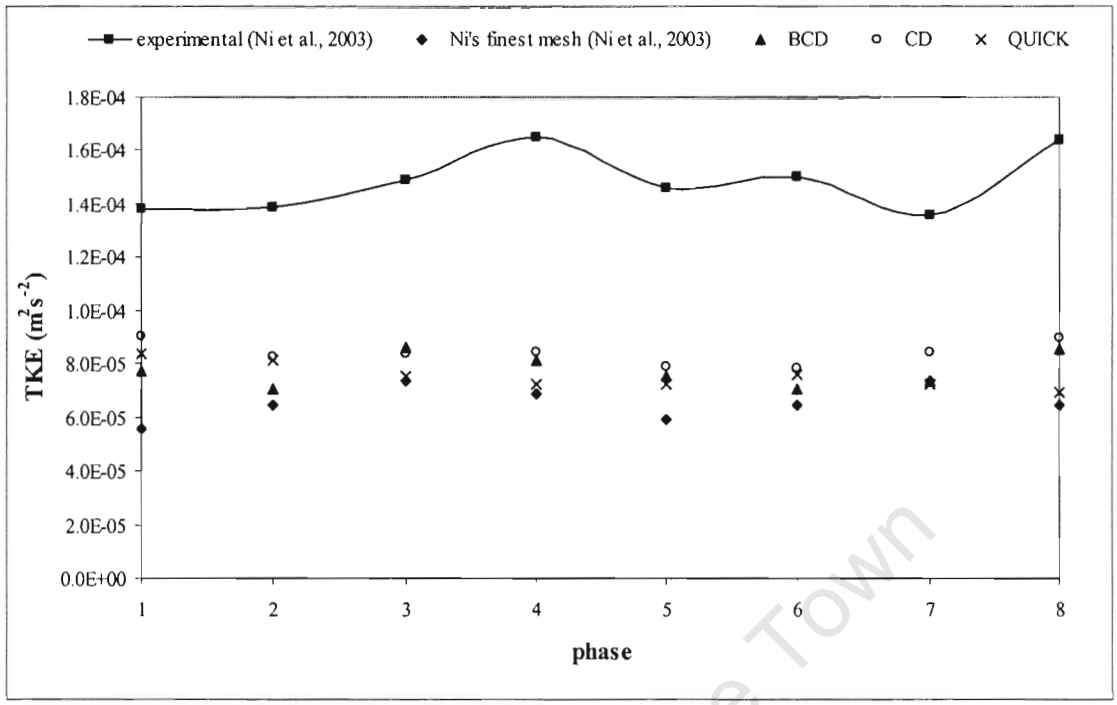

(a)

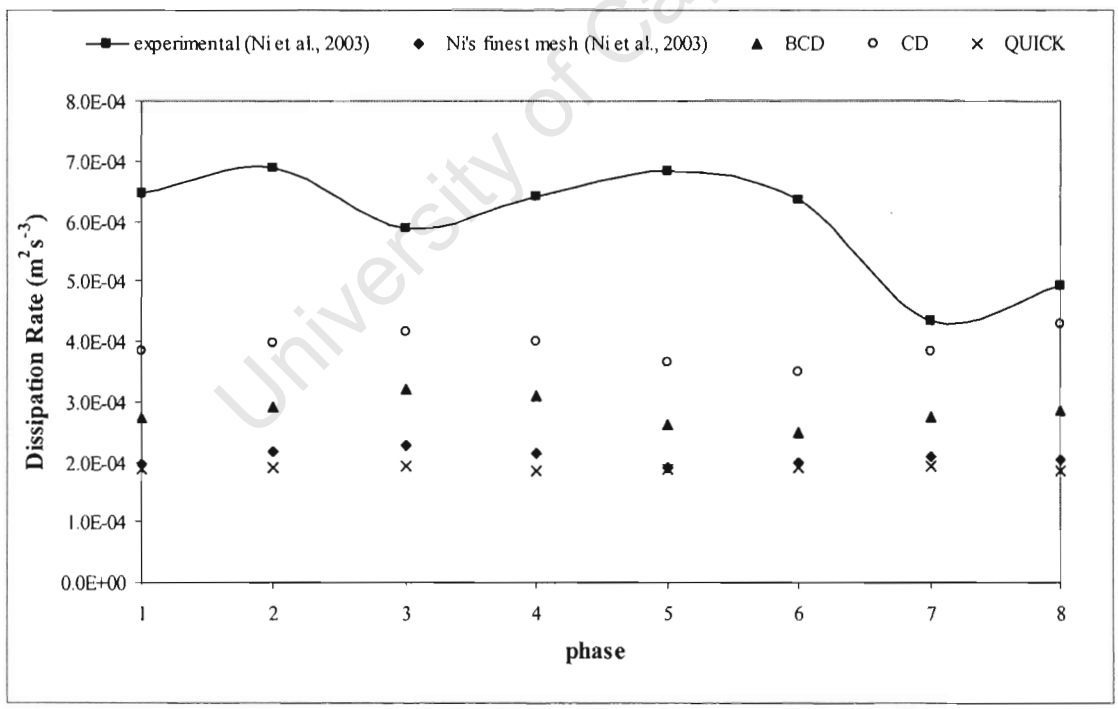

(b)

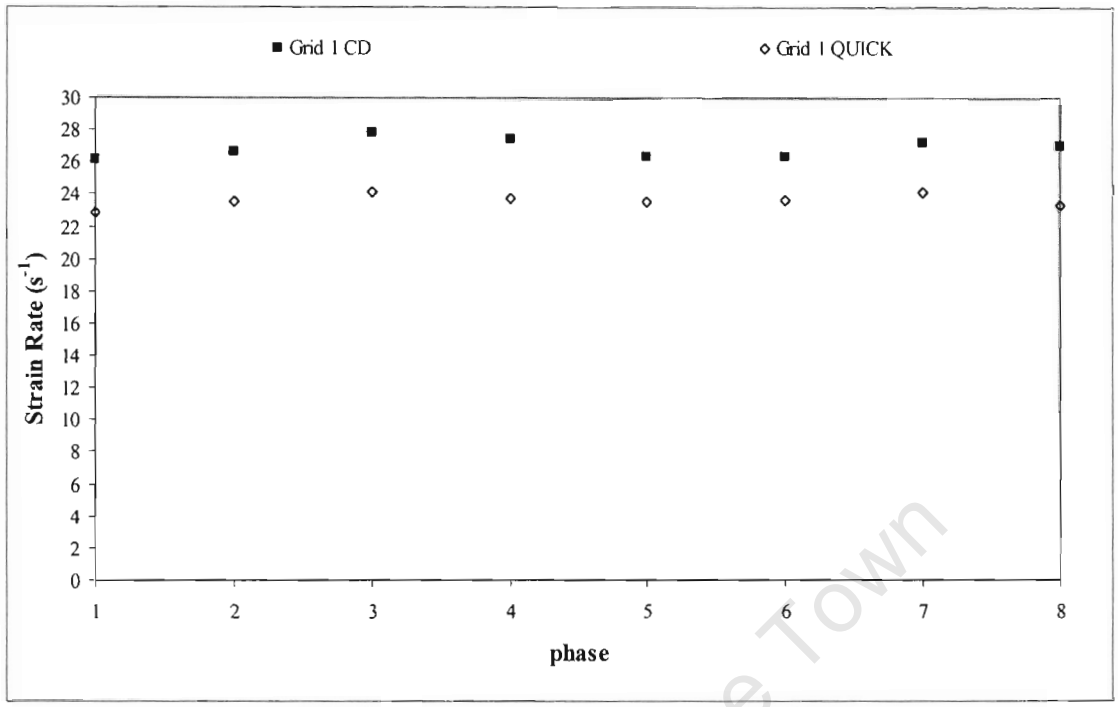

(c)

Figure 7-8. Graphs of phase averaged (a) turbulent kinetic energy, (b) dissipation rate and (c) strain rate comparing different momentum discretization schemes (f = 1Hz, x_o = 4mm)

7.5.3 Pressure Discretization Schemes

The effect of using the PRESTO! Pressure discretization scheme was investigated using grid 1 together with the other modelling options decided before, namely the dynamic Smagorinsky-Lilly subgrid scale model, the SIMPLEC pressure-velocity coupling and the QUICK momentum discretization scheme. The flow after 5 cycles looked almost identical to the flow when using the Standard scheme, apart from the fact that the velocity magnitude around the right hand set of vortices was higher when using PRESTO!. When results were sampled over the same cycles as before, the results of both turbulent kinetic energy and dissipation rate were far higher than when using the standard scheme. It was noted that the volume averaged velocity magnitude was not the same during each cycle. This would cause the TKE, which is defined as half the square of the fluctuating part of the velocity, to be unrealistically large, since there was a large velocity fluctuation when compared to other cycles.

It is uncertain why the flow using PRESTO! remains statistically transient for longer than when using the Standard scheme, but after 7 cycles the volume averaged velocity magnitude became equal over subsequent cycles. Results after this point showed that both TKE and dissipation rate were similar to the results obtained using the Standard scheme, as can be seen in Fig. 7-9a and b.

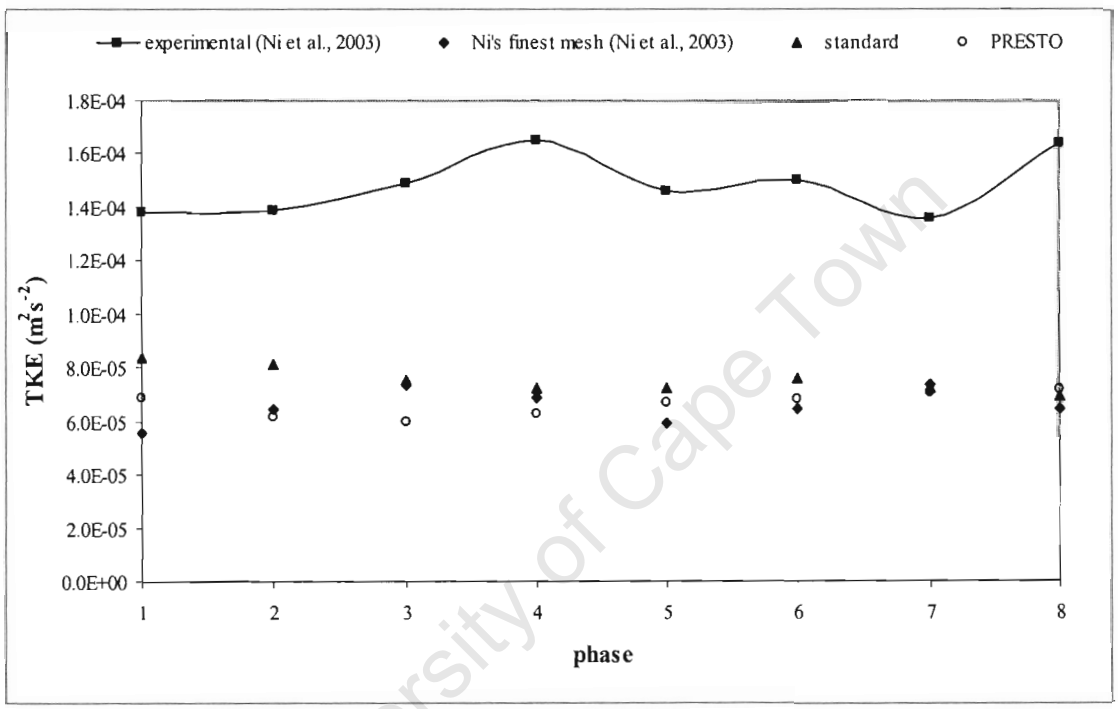

(a)

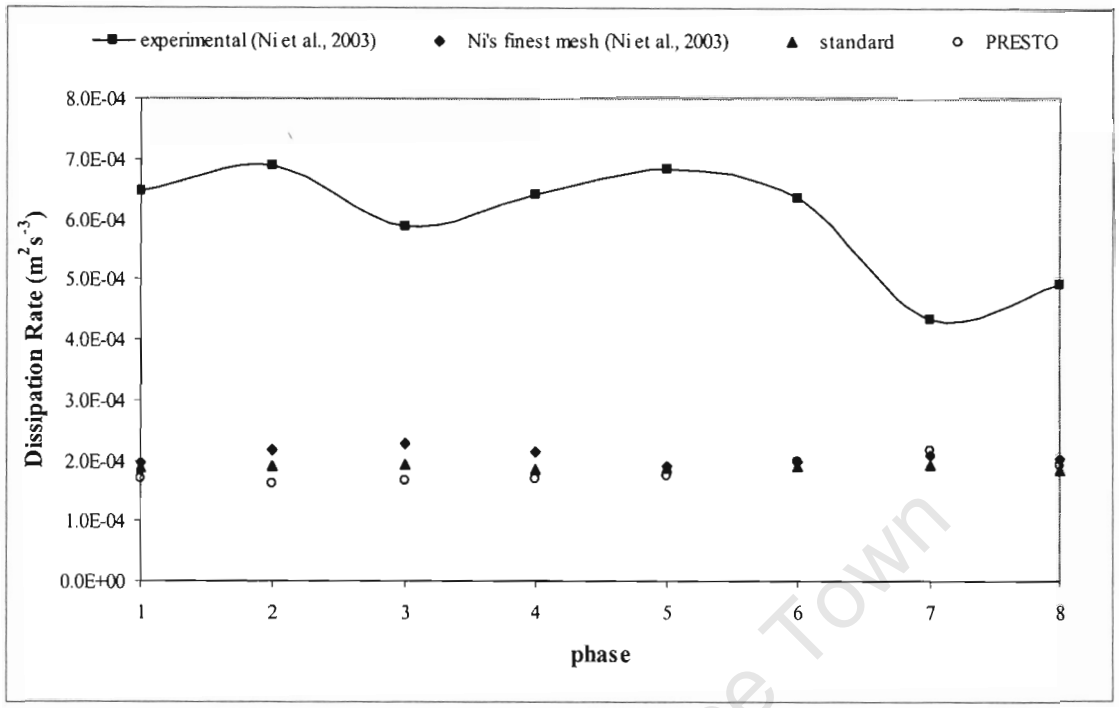

(b)

Figure 7-9. Graphs of phase averaged (a) turbulent kinetic energy and (b) dissipation rate comparing different pressure discretization schemes (f = 1Hz, x_o = 4mm)

7.6 Fine Grid Simulations

Using the Dynamic Smagorinsky-Lilly subgrid-scale model, the SIMPLEC pressure-velocity coupling and the Standard pressure discretization scheme, simulations were then conducted together with grid 3 over 15 cycles, with results averaged over the last 4 cycles. Results were only averaged over these cycles since the mean velocity magnitude was still differing between cycles in preceding cycles, and only after the 11^{th} cycle did it begin to repeat over cycles. Both the QUICK and Central Differencing momentum discretization scheme were investigated using this grid. Like the simulations conducted with grid 1, the Central Differencing scheme predicted that the flow became asymmetric far earlier than predicted by the QUICK scheme, with the simulation using the Central Differencing scheme becoming asymmetric during the 3^{rd} cycle, whereas, the QUICK scheme predicted asymmetry after 8 cycles.

Results of phase averaged velocity magnitude using both momentum discretization schemes are almost identical to results using grid 1, and phase averaged TKE from both schemes are also in the same range, as can be seen in Fig. 7-10a. There is a large difference in the results of phase averaged dissipation rate between the Central Differencing and QUICK schemes however, as found before. The different grids predicted almost the same results when the same momentum discretization scheme was used, as is seen in Fig. 7-10b.

The fact that the results from both the coarsest grid of 551 225 cells and the finest grid of 726 804 cells predicted results with minimal difference between them indicates that the model was in fact grid independent when using the coarsest grid. It is thought that the small difference is only because of insufficient mesh refinement in certain area of high velocity.

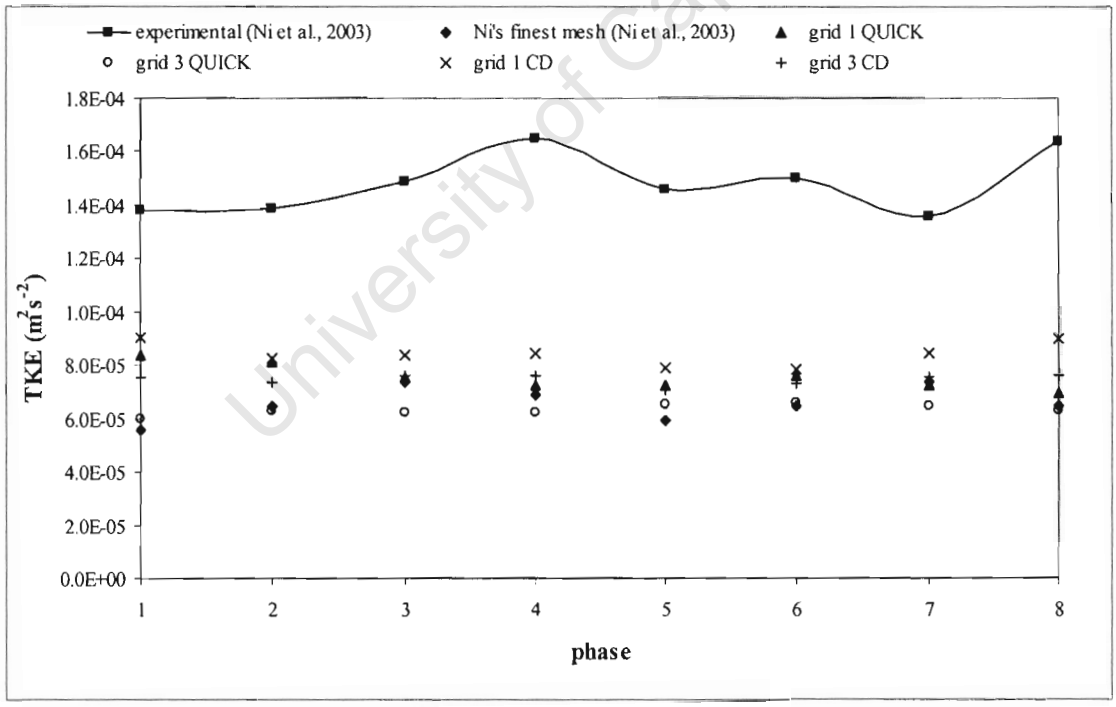

(a)

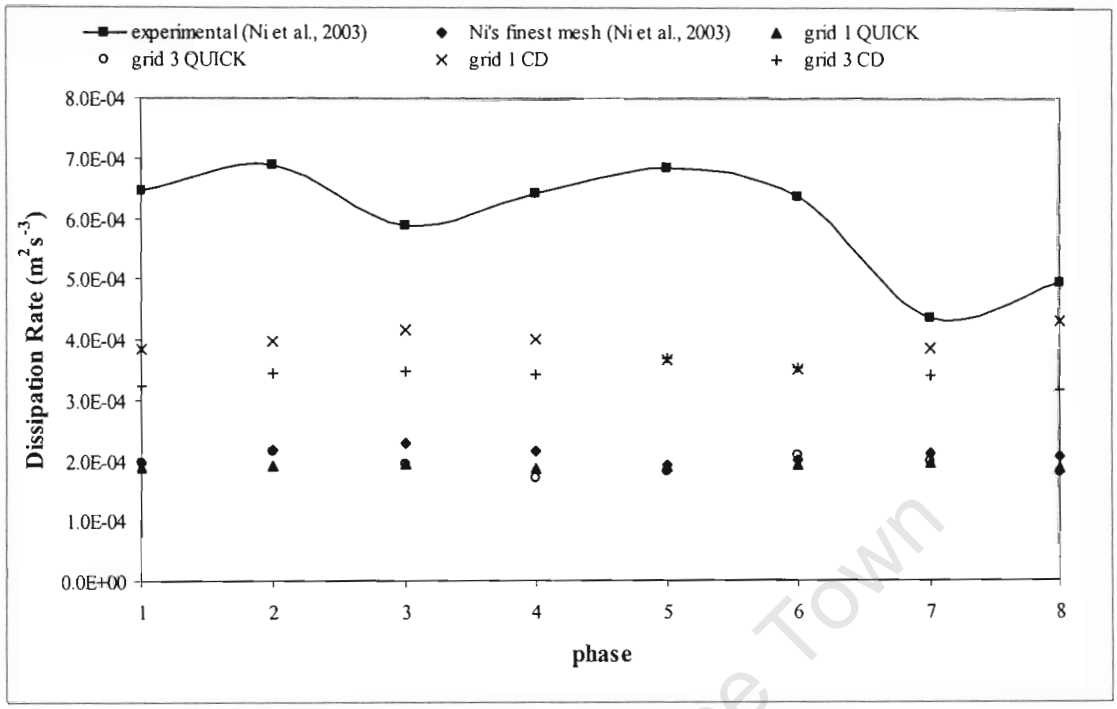

(b)

Figure 7-10. Graphs of phase averaged (a) turbulent kinetic energy and (b) dissipation rate comparing different pressure discretization schemes (f = 1Hz, x_o = 4mm)

8. Conclusions

The aim of this research was to develop a numerical model to accurately predict the flow in an Oscillatory Baffled Column. Comparisons of different methods of defining the oscillatory flow were made. The effects of different grid sizes and discretization schemes were also investigated.

The following conclusions were drawn:

8.1 Boundary Conditions

The most accurate boundary conditions that were investigated to define the oscillatory flow were found to be translational periodic boundaries together with a journal file to define the sinusoidally oscillating flow. It was found that the use of a velocity inlet did not allow the turbulent flow to develop and therefore predicted considerably lower volume averaged velocity magnitudes and turbulent kinetic energy

8.2 LES versus RANS turbulence model

From literature it is known that RANS turbulence models that employ the Boussinesq hypothesis are not appropriate for modelling the flow in OBC's. It was found that Large Eddy Simulation predicted phase averaged mean velocity magnitudes that were close to experimentally calculated values. Although predicted values of phase averaged mean turbulent kinetic energy and energy dissipation rate were not close to experimental results, they were in a realistic range. LES was therefore used throughout this research, and was found to be less computationally expensive than the Reynolds Stress turbulence model. It was found that there were no significant differences between different subgrid scale models used, so the Dynamic Smagorinsky Lilly subgrid-scale model was chosen to be used because of potential increases in accuracy when used for different Re_o numbers.

8.3 Computational Grid

From an initial grid independence study, it was found that a grid of 726 804 cells predicted results of phase averaged turbulent kinetic energy and integral length scale that were closer to experimental results than grids of 627 776 and 551 225 cells. When the chosen discretization and subgrid-scale models were used however, the results from the coarsest and finest grids were almost the identical, indicating grid independence. It is therefore thought that grid 3 was adequate to create a grid independent numerical model of the OBC at the Re_o investigated.

8.4 Discretization Schemes

Various discretization schemes were investigated and the following was found:

- The SIMPLEC was found to be the most appropriate pressure-velocity coupling discretization scheme to model the OBC using LES.
- The Central Differencing momentum discretization scheme predicted a flow that became asymmetric during the 3rd cycle, whereas the QUICK scheme predicted a change to asymmetry after 8 cycles. Other research (2004CH01) indicated that this change only occurs around the same time that the QUICK scheme predicts, and it was therefore chosen as the most appropriate momentum discretization scheme.
- It was found that the PRESTO! scheme predicted a longer time for the flow to stabilize, but once this had occurred, there was no significant difference in the predicted flows when using the Standard or PRESTO! Schemes. The Standard pressure discretization scheme was therefore chosen as the most appropriate scheme to use.
- The discretization schemes had no significant effect on the phase averaged mean velocity once the flow had stabilized, but did effect the time taken for the flow to stabilize.
- Only the momentum discretization had any significant effect on the predicted flow, whereas the pressure-velocity coupling and pressure discretization schemes had little or no effect.

It was observed that although phase averaged mean velocity magnitudes were the same for all different modelling parameters investigated, the flow that was predicted was not the same. The amount of asymmetry in the flow differed, and vortices were in different positions. This indicates that the form of the experimental data was not ideal for validation purposes, since not only was the data phase averaged, but also volume averaged, thereby aggregating a large amount of data into only one value. Unfortunately, due to the chaotic, asymmetric nature of the flow inside OBC's, it is unlikely that the local flow variables will ever be equal at the same phase over successive cycles.

Using volume averaged results of DPIV data is also a possible cause of discrepancy between numerical and experimental results since the experimental DPIV data does not include the 3mm area along the walls when volume averaging the results, which is the area of highest strain rate. Due to the fact that the data is only 2d, volume averaged results have to be interpolated from this. Therefore it is thought that the most appropriate form of data for comparison would be in the form of phase averaged but not volume averaged data. Plots of the variables along the diameter or the length of the OBC could then be investigated, thereby comparing both the magnitude of the variable, as well as the spatial distribution.

9. Recommendations

TKE Calculation

During this research, an external FORTRAN program was written to calculate the phase averaged mean TKE. Because of this, the local TKE values were not known. In order to obtain this information, a user defined function needs to be written in C so that the TKE can be calculated directly in FLUENT, and therefore contour plots could also be made of the TKE. This will help in future research when investigating the effect of different combinations of oscillation frequency and amplitude on the local distribution of TKE and energy dissipation rate.

Model Geometry

Rather than using a numerical model geometry with 3 full inter-baffle cells modeled, it was thought that a more appropriate geometry would be to model one full inter-baffle cell and then two halves on either side (see fig. 11.1). Since translational periodic boundaries are used, this should be more realistic, since the periodic boundaries would be in a position where the flow is periodic in reality, rather than in the model geometry used before, where the boundaries are in positions where there is actually no periodic flow in reality

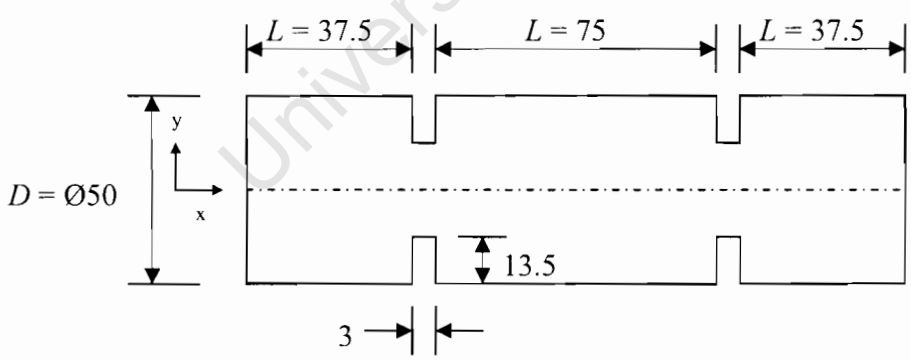

Figure 9-1. Dimensions of baffled column using half length side baffled cells (All dimensions in mm)

10. List of References

[2004FL01] Fluent 6.2.16 Users Guide, *Fluent Inc.,* 2004

[1989 BR01] Brunold, C.R., Hunns, J.C.B., Mackley, M.R., & Thompson, J.W., Experimental observations on flow patterns and energy losses for oscillatory flow in ducts containing sharp edges. *Chemical Engineering Science*, Vol. 44, pp. 1227-1244, 1989.

[1991MA01] Mackley, M.R., & Ni, X., Mixing and dispersion in a baffled tube for steady laminar and pulsative flow. *Chemical Engineering Science,* Vol. 46, No. 12, pp. 3139-3151, 1991.

[1991WH01] White, F.M., Viscous Fluid Flow, 2nd Ed, McGraw Hill Inc., 1991.

[1995VE01] Versteeg, H.K., Malalasekera, W., An introduction to computational fluid dynamics, The finite volume method, Pearson Prentice Hall, 1995.

[1996RO01] Roberts, E.P.L., & Mackley, M.R., The development of asymmetry and period doubling for oscillatory flow in baffled channels. *Journal of Fluid Mechanics*, Vol. 328, pp. 19-48, 1996.

[1995WI01] Wilcox, David C., Turbulence Modelling for CFD, 2nd Ed., DCW Industries, 1995.

[1999SH01] Schubert, H., On the turbulence-controlled microprocesses in flotation machines, *Int. J. Miner. Process.,* Vol. 56, pp. 257-276, 1999.

[2000NI01] Ni, X., Cosgrove, J.A., Arnott, A.D., Greated, C.A., & Cumming, R.H., On the measurement of strain rate in an oscillatory baffled column using particle image velocimetry. *Chemical Engineering Science*, Vol. 55, pp. 3195-3208, 2000.

[2003FI01] Fitch, A.W., & Ni, X., On the determination of axial dispersion coefficient in a batch oscillatory baffled column using laser induced fluorescence. *Chemical Engineering Journal,* Vol. 92, pp. 243-253, 2003.

[2003JI01] Jian, H., Ni, X., On modelling turbulent flow in an oscillatory baffled column – RANS model or large-eddy simulation. *Journal of Chemical Technology and Biotechnology,* Vol. 78, pp. 321-325, 2003.

[2003NI01] Ni, X., Jian, H., & Fitch, A.W., Computational fluid dynamic modelling of flow patterns in an oscillatory baffled column. *Chemical Engineering Science,* Vol. 57, pp. 2849-2862, 2002.

[2003NI01] Ni, X., Jian, H., & Fitch, A.W., Evaluation of turbulent integral length scale in an oscillatory baffled column using large eddy simulation and digital particle image velocimetry. *Trans IChemE, part A,* Vol. 81, pp. 842-853, 2003.

[2004CH01] Chew, C.M., Ristic, R.I., Reynolds, G.K., Ooi, R.C., Characterization of impeller driven and oscillatory mixing by spatial and temporal shear rate distributions. *Chemical Engineering Science,* Vol. 59, pp. 1557-1568, 2004.

Appendix 1 - Reynolds Stress Model Transport Equations

FLUENT uses the following equations as the RSM transport equations (2004FL01)

$$\frac{\partial}{\partial t}\left(\rho\overline{u_i'u_j'}\right)+\frac{\partial}{\partial x_k}\left(\rho u_k\overline{u_i'u_j'}\right)=-\frac{\partial}{\partial x_k}\left[\rho\overline{u_i'u'u_k'}+\overline{p\left(\delta_{kj}u_i'+\delta_{ik}u_j'\right)}\right]+\frac{\partial}{\partial x_k}\left[\mu\frac{\partial}{\partial x_k}\overline{u_i'u_j'}\right]$$

Time derivative | C_{ij} Convection | $D_{T,ij}$ Turbulent diffusion | $D_{L,ij}$ Molecular diffusion

$$-\rho\left(\overline{u_i'u_k'}\frac{\partial u_j}{\partial x_k}+\overline{u_j'u_k'}\frac{\partial u_i}{\partial x_k}\right)-\rho\beta\left(g_i\overline{u_j'\theta}+g_j\overline{u_i'\theta}\right)+p\left(\frac{\partial\overline{u_i}}{\partial x_j}+\frac{\partial\overline{u_j}}{\partial x_i}\right)-2\mu\frac{\partial u_i'}{\partial x_k}\frac{\partial\overline{u_j}}{\partial x_k}$$

P_{ij} Stress Production | G_{ij} Buoyancy Production | ϕ_{ij} Pressure Strain | ε_{ij} Dissipation

$$-2\rho\Omega_k\left(u_j'u_m'\varepsilon_{ikm}+u_j'u_m'\varepsilon_{jkm}\right)+S_{user}$$

F_{ij} Production by System Rotation | User defined source term

The terms that are modeled are $D_{T,ij}$, G_{ij} , ϕ_{ij} and ε_{ij}.

- Turbulent Diffusion: $D_{T,ij}=\frac{\partial}{\partial x_k}\left(\frac{\mu_t}{\sigma_k}\frac{\partial\overline{u_i'u_j'}}{\partial x_k}\right)$ where σ_k = 0.82

- Pressure Strain: $\phi_{ij}=\phi_{ij,1}+\phi_{ij,2}+\phi_{ij,w}$

  where

  $$\phi_{ij,1}=-C_1\rho\frac{\varepsilon}{k}\left[\overline{u_i'u_j'}-\frac{2}{3}\delta_{ij}k\right] \qquad C_1 = 1.8$$

  $$\phi_{ij,2}=-C_2\left[\left(P_{ij}+F_{ij}+G_{ij}-C_{ij}\right)-\frac{2}{3}\delta_{ij}\left(P+G-C\right)\right]$$

where $C_2 = 0.6$, $P = \frac{1}{2}P_{kk}$, $G = \frac{1}{2}G_{kk}$, $C = \frac{1}{2}C_{kk}$

$$\phi_{ij,w} = C_1' \frac{\varepsilon}{k}\left(\overline{u_k' u_m'} n_k n_m \delta_{ij} - \frac{3}{2}\overline{u_i' u_k'} n_j n_k - \frac{3}{2}\overline{u_j' u_k'} n_i n_k\right)\frac{k^{3/2}}{C_\ell \varepsilon d}$$

$$+C_2'\left(\phi_{km,2} n_k n_m \delta_{ij} - \frac{3}{2}\phi_{ik,2} n_j n_k - \frac{3}{2}\phi_{jk,2} n_i n_k\right)\frac{k^{3/2}}{C_\ell \varepsilon d}$$

where $C_1' = 0.5$, $C_2' = 0.3$, n_k is the x_k component of the unit normal to the wall, d is the normal distance to the wall, and $C_\ell = \frac{C_\mu^{3/4}}{\kappa}$, where C_μ = 0.09 and κ is the von Kármán constant (0.4187)

- Buoyancy production: $G_{ij} = \frac{\mu_t}{\rho \Pr_t}\left(g_i \frac{\partial \rho}{\partial x_j} + g_j \frac{\partial \rho}{\partial x_i}\right)$

where $\Pr_t$ is the turbulent Prandtl number for energy (0.85)

- Dissipation: $\varepsilon_{ij} = \frac{2}{3}\delta ij\left(\rho\varepsilon + 2\rho\varepsilon M_t^2\right)$ where $M_t = \sqrt{\frac{k}{a^2}}$, a being the speed of sound.

The scalar values of k and ε in the above equations are calculated using the same model transport equations as used in the $k-\varepsilon$ turbulence model (See Fluent 6.2.16 Users guide for more information)

Appendix 2 – Journal file Used to Define Periodic Oscillatory Mass Flow Rate

```
;;journal file to set sinusoidally oscillating periodic mass flow
(define pi 3.1415926)
(define t (rpgetvar 'flow-time))
(display t)
(define m (* 0.04926 (cos (* 2 (* pi t)))))
(display m )
(ti-menu-load-string(format #f "define/periodic-conditions/massflow-rate-specification ~d" m))
```

Appendix 3 – Fortran Code to Calculate Turbulent Kinetic Energy

```
!    Last change:  C    23 Aug 2005    2:41 pm
!-----------------------------------------------------------------------
! file:       phase-averager_v3.f90
! programmer:  C. Bakker              date: june 2005
! language:    Lahey fortran 90
! NOTE:
! * FLUENT must be run with LINUX when exporting files in order for
!   program to work.
! * Manually export file named "volume" of cell volumes into same directory
!
!-----------------------------------------------------------------------
MODULE working_routines

CONTAINS

!-----------------------------------------------------------------------
! subroutine:   file_length
! purpose:      determines number of lines in any file
! programmer:   C. Bakker              date: 1 June 2005
! language:     Lahey fortran 90
! ARGUMENTS:
! CHECK         in      contains name of input file
! LENGTH        out     contains length of input file
!-----------------------------------------------------------------------

SUBROUTINE file_length(check,length)
IMPLICIT NONE
INTEGER :: ios=0
INTEGER, INTENT(OUT)::length
INTEGER, PARAMETER :: in=4
CHARACTER(LEN=72) :: temp
CHARACTER(LEN=24), INTENT(IN) :: check

length=0

OPEN(UNIT=IN, FILE=check, STATUS="old", IOSTAT=ios)

IF (ios/=0) THEN
 WRITE(*,*)'The file cannot be opened - aborting program!'
 STOP

ELSE
 REWIND(IN)
 WRITE(*,*)'checking length of file'
  READ(UNIT=IN,FMT=900) temp
  WRITE(*,*)temp
 DO
   READ(UNIT=IN,FMT=900,IOSTAT=ios) temp
   if (ios==0) then
     length = length+1

   else
     exit
   end if
 END DO
END IF

REWIND(IN)

WRITE(*,*)'length of file is:  ',length
900 FORMAT(a134)

RETURN
END SUBROUTINE file_length

!-----------------------------------------------------------------------
! subroutine:   only_vols
! purpose:      creates file "cell-vol" with only cell volume of each cell
! programmer:   C. Bakker              date: 1 June 2005
! language:     Lahey fortran 90
! ARGUMENTS:
! length        in      contains length of file
! cell-vol              output file containing cell volumes
!-----------------------------------------------------------------------
SUBROUTINE only_vols(length)
IMPLICIT NONE
INTEGER :: IN=9,OUT=10,i=0,ios=0
INTEGER, INTENT(IN) :: length
CHARACTER(LEN=72) :: temp

OPEN(UNIT=IN, FILE='volume', STATUS="old", IOSTAT=ios)

OPEN(UNIT=OUT,FILE='cell-vol',STATUS="replace")
REWIND(OUT)
```

```
IF (ios/=0) THEN
 WRITE(*,*)'The file cannot be opened - aborting program!'
 STOP
ELSE
 REWIND(IN)

  READ(UNIT=IN,FMT=900) temp
 DO i=1,(length-1)
   READ(UNIT=IN,FMT=900,IOSTAT=ios) temp
   if (ios==0) then
     WRITE(UNIT=out,FMT=*) temp
   else
     exit
   end if
 END DO
END IF

REWIND(IN)
REWIND(OUT)

900 FORMAT(a134)
return
END subroutine only_vols

!_____________________________________________________________________
! subroutine:   cell_vol
! purpose:      creates array of cell volumes
! programmer:   C. Bakker              date: 1 June 2005
! language:     Lahey fortran 90
! ARGUMENTS:
! length        in     length of file
! vol           out    array of cell volumes
!_____________________________________________________________________
subroutine cell_vol(length,vol)
implicit none
INTEGER :: IN=10,i=0
INTEGER, INTENT(IN) :: length
REAL(8), DIMENSION(length-1), INTENT(OUT) :: vol

OPEN(UNIT=in,FILE='cell-vol',STATUS="old")
REWIND(in)

do i=1,(length-1)
READ(UNIT=IN,FMT=*)vol(i)
end do

return
END subroutine cell_vol



!_____________________________________________________________________
! subroutine:  concatenate
! purpose:     makes file name to read by adding timestep number to end of file name
! programmer:  C. Bakker            date: 1 June 2005
! language:    Lahey fortran 90
! ARGUMENTS:
! file_name    in    group name of the input files
! file_number  in    number of the file
! in_file      out   concatenated file name
! begin        in    number of timestep where sampling begins
!_____________________________________________________________________
SUBROUTINE concatenate(file_name,file_number,in_file,begin)
implicit none
INTEGER, INTENT(IN) :: file_number,begin
CHARACTER(LEN=24), INTENT(IN) :: file_name
CHARACTER(LEN=24) :: num
CHARACTER(LEN=24), INTENT(OUT) :: in_file
INTEGER, PARAMETER :: out=6,IN=6

OPEN(UNIT=out, FILE="temp_file.inp", STATUS="replace")
REWIND(OUT)

WRITE(UNIT=out,FMT=*)(file_number-1)*25+begin

OPEN(UNIT=IN, FILE="temp_file.inp", STATUS="OLD")

  REWIND(IN)

  READ(UNIT=IN,FMT=*)num

in_file = TRIM(file_name)//num

 return
end subroutine concatenate
```

```
!_____________________________________________________________________
! subroutine:   space_remove
! purpose:      removes spaces in front of data
! programmer:   C. Bakker              date: 1 June 2005
! language:     Lahey fortran 90
! ARGUMENTS:
! in_file       in      data file name
!_____________________________________________________________________

SUBROUTINE space_remove(in_file)
IMPLICIT NONE
INTEGER :: ios=0
INTEGER, PARAMETER :: in=4,OUT=7
CHARACTER(LEN=72) :: temp
CHARACTER(LEN=24), INTENT(IN) :: in_file

OPEN(UNIT=IN, FILE=in_file, STATUS="old", IOSTAT=ios)

OPEN(UNIT=OUT,FILE='no_gaps.inp',STATUS="replace")
REWIND(OUT)

IF (ios/=0) THEN
 WRITE(*,*)'The file cannot be opened - aborting program!'
 STOP
ELSE
 REWIND(IN)

  READ(UNIT=IN,FMT=900) temp
 DO
   READ(UNIT=IN,FMT=900,IOSTAT=ios) temp
   if (ios==0) then
     WRITE(UNIT=out,FMT=*) temp
   else
     exit
   end if
 END DO
END IF

REWIND(IN)
REWIND(OUT)

900 FORMAT(a134)
RETURN
END SUBROUTINE space_remove

!_____________________________________________________________________
```

```
! subroutine:   reading
! purpose:      reads the file and solves for phase averaged velocity
! programmer:   C. Bakker              date: 1 June 2005
! language:     Lahey fortran 90
! ARGUMENTS:
! i                       in      file number
! in_file       in      data file name
! length        in      length of data file
! velocity      out     array containing phase averaged velocity
! tke           out     array containing phase averaged tke
!_____________________________________________________________________
SUBROUTINE reading(i,in_file,length,phase,velocity,tke)
IMPLICIT NONE
INTEGER, intent(IN) :: i
INTEGER :: counter=0,cyc_no=0
INTEGER, INTENT(IN) :: length
INTEGER, INTENT(OUT) :: phase
INTEGER, PARAMETER :: in=7,OUT=9
CHARACTER(LEN=24), INTENT(IN) :: in_file
REAL(8) :: init_vel=0.,temp_tke=0.
REAL(8), DIMENSION(8,(length-1)) :: vel,tke_array,vel_sqd
REAL(8),DIMENSION(8,(length-1)), INTENT(OUT) ::velocity,tke

phase = MOD(i,8)

if (phase==0) then
phase=8
END if
cyc_no = (i+(8-phase))/8
WRITE(*,*)'cycle:  ', cyc_no

OPEN(UNIT=IN, FILE='no_gaps.inp', STATUS="OLD")
REWIND(IN)
WRITE(*,*) 'reading file:   ' ,in_file

OPEN(UNIT=OUT,FILE='turbulent ke.txt',STATUS="replace")
REWIND(OUT)
  do counter=1,(length-1)
    READ(UNIT=IN,FMT=*)init_vel
    vel(phase,counter) = vel(phase,counter) + init_vel
    vel_sqd(phase,counter) = vel_sqd(phase,counter) + (init_vel**2)
  end do

  velocity = vel/cyc_no

  counter=0
```

```
  REWIND(IN)

  do counter = 1,(length-1)
    READ(UNIT=IN,FMT=*)init_vel
    temp_tke = ABS(0.5*((vel_sqd(phase,counter))/cyc_no-
(velocity(phase,counter))**2))
    tke_array(phase,counter) = tke_array(phase,counter) + temp_tke
    WRITE(UNIT=out,FMT=901)temp_tke

  end do

  tke = tke_array/cyc_no

901 format (E19.9)

return
END subroutine reading

END module working_routines

!_____________________________________________________________
! program:     driver
! purpose:     writes file "output.csv" containing phase ave vel and TKE
! programmer:  C. Bakker            date: 1 June 2005
! language:    Lahey fortran 90
!_____________________________________________________________

PROGRAM driver
USE working_routines
implicit none
INTEGER :: i=0,OUT=8,phase=0,counter=0,c=0
INTEGER :: cycles=0,n=0,length=0,begin=0
CHARACTER(LEN=24) :: file_name,check,in_file
REAL :: tot_vol=0.,vol_check=0.
REAL(8), DIMENSION(8) :: tot_vel=0.,tot_tke=0.
REAL(8),DIMENSION(:,:),allocatable :: velocity,tke
REAL(8), DIMENSION(:), ALLOCATABLE :: vol

WRITE(*,*) 'program that solves for phase averaged TKE'
WRITE(*,*) 'enter name of first file:   '
READ(*,*) check
WRITE(*,*) 'enter group name of files:   '

READ(*,*) file_name
WRITE(*,*)  'enter number of cycles that sim runs for:   '
READ(*,*) cycles

WRITE(*,*)'what timestep number must sampling be started:  '
READ(*,*)begin

tot_vol = 0.0001470527

CALL file_length(check,length)

CALL only_vols(length)

ALLOCATE (vol(length-1))

CALL cell_vol(length,vol)

ALLOCATE (velocity(8,(length-1)))
ALLOCATE (tke(8,(length-1)))

DO i=1,(cycles*8)

CALL concatenate(file_name,i,in_file,begin)
WRITE(*,*)'concatenated    ', in_file

CALL space_remove(in_file)
 WRITE(*,*)'removed leading spaces on    ', in_file

CALL reading(i,in_file,length,phase,velocity,tke)

WRITE(*,*) 'writing to phase:  ', phase

END DO

do c=1,8
 vol_check=0.
 do counter=1,(length-1)
  tot_vel(c)=tot_vel(c) + (velocity(c,counter) * (vol(counter)/tot_vol))
  tot_tke(c)=tot_tke(c) + (tke(c,counter) * (vol(counter)/tot_vol))
  vol_check=vol_check + vol(counter)
 end do
 WRITE(*,*)'volume check: ', vol_check
  WRITE(*,905)tot_vel(c)
end do

OPEN(UNIT=OUT,FILE='output.csv',STATUS='replace')
REWIND(OUT)
```

```
WRITE(UNIT=out,FMT=900)

do n=1,8
WRITE(UNIT=out,FMT=903) n,tot_vel(n), tot_tke(n)
end do

900 FORMAT("phase, VELOCITY, TKE")
903 FORMAT(" ",I1,",",E15.9,",",E15.9)
905 format (E15.9)
stop
end program driver
```